AFOSR-TR- 86-0055

FINAL TECHNICAL REPORT

1 July 1983 - 1 October 1984

ARPA Order Number:	4770
Program Code:	3D60
Name of Contractor:	Columbia University in the City of New York
Effective Date of Contract:	1 July 1983
Contract Expiration Date:	30 June 1984
Amount of Contract:	$74,982
Principal Investigator:	Tracy L. Johnson
Program Manager & Phone No.:	Dr. Henry Radoski 202-767-4906
Short Title of Work:	Measurement of Elastic Properties and Static Strength

The views and conclusions contained in this document are those of the authors and should not be interpreted as necessarily representing the official policies, either expressed or implied, of the Defense Advanced Research Projects Agency or the U.S. Government

Sponsored by
Advanced Research Projects AGency (DOD)
ARPA Order No. 4770
Monitored by AFOSR Unde Contract #F49620-83-C-0124

Lamont-Doherty Geological Observatory of Columbia University
Palisades, New York 10964

October 1984

UNCLASSIFIED

SECURITY CLASSIFICATION OF THIS PAGE

AD-A166 155

REPORT DOCUMENTATION PAGE

1a. REPORT SECURITY CLASSIFICATION: Unclassified	1b. RESTRICTIVE MARKINGS
2a. SECURITY CLASSIFICATION AUTHORITY	3. DISTRIBUTION/AVAILABILITY OF REPORT: Approved for public release; distribution unlimited.
2b. DECLASSIFICATION/DOWNGRADING SCHEDULE	
4. PERFORMING ORGANIZATION REPORT NUMBER(S)	5. MONITORING ORGANIZATION REPORT NUMBER(S): AFOSR-TR- 86-0055 N/A
6a. NAME OF PERFORMING ORGANIZATION: Columbia University; 6b. OFFICE SYMBOL (If applicable):	7a. NAME OF MONITORING ORGANIZATION: AFOSR
6c. ADDRESS (City, State and ZIP Code): Lamont-Doherty Geological Observatory of Columbia University Palisades, NY 10964	7b. ADDRESS (City, State and ZIP Code): Building 410 Bolling AFB, DC 20332-6448
8a. NAME OF FUNDING/SPONSORING ORGANIZATION: AFOSR; 8b. OFFICE SYMBOL (If applicable): NP	9. PROCUREMENT INSTRUMENT IDENTIFICATION NUMBER: F49620-83-C-0124
8c. ADDRESS (City, State and ZIP Code): Building 410 Bolling AFB, DC 20332-6448	10. SOURCE OF FUNDING NOS.

PROGRAM ELEMENT NO.	PROJECT NO.	TASK NO.	WORK UNIT NO.
61102F	2311	A1	N/A

11. TITLE (Include Security Classification): "MEASUREMENT OF ELASTIC PROPERTIES AND STATIC STRENGTH"

12. PERSONAL AUTHOR(S): Dr T L. Johnson

13a. TYPE OF REPORT	13b. TIME COVERED	14. DATE OF REPORT (Yr., Mo., Day)	15. PAGE COUNT
FINAL	FROM 83/07/01 TO 84/10/01	84/10/01	49

16. SUPPLEMENTARY NOTATION

17. COSATI CODES			18. SUBJECT TERMS (Continue on reverse if necessary and identify by block number)
FIELD	GROUP	SUB. GR.	

19. ABSTRACT (Continue on reverse if necessary and identify by block number)

Initial effort supported by the contract was mainly devoted to obtaining and preparing samples of Westerly granite for experiments. Preliminary experiments to characterize the properties of Westerly granite were performed on small samples obtained from the Bonner Monument Company. Material properties measured agreed well with previous determinations.

20. DISTRIBUTION/AVAILABILITY OF ABSTRACT	21. ABSTRACT SECURITY CLASSIFICATION
UNCLASSIFIED/UNLIMITED ☐ SAME AS RPT. ☒ DTIC USERS ☐	UNCLASSIFIED

22a. NAME OF RESPONSIBLE INDIVIDUAL	22b. TELEPHONE NUMBER (Include Area Code)	22c. OFFICE SYMBOL
HENRY R. RADOSKI	202/767-4906	NP

DD FORM 1473, 83 APR EDITION OF 1 JAN 73 IS OBSOLETE.

UNCLASSIFIED

SECURITY CLASSIFICATION OF THIS PAGE

TABLE OF CONTENTS

	Page
INTRODUCTION	1
OVERVIEW	1
EXPERIMENTAL RESULTS - WESTERLY GRANITE	4
EXPERIMENTAL RESULTS - SIERRA WHITE GRANITE	13
Individual Experiments	15
Conclusion	16
REFERENCES	18
TABLES	19
FIGURES	22

INTRODUCTION

The prediction of seismic coupling for nuclear monitoring requires theoretical models capable of calculating ground motions. The models must have a sound physical basis and be able to represent dynamic material behavior near the source.

This portion of the study of stress wave propagation in low porosity rock is aimed at determining quasi-static properties of rock necessary to use in numerical models predicting wave propagation. Further, the failure process of low porosity rock under simulated shock loading is being studied to establish the failure mechanisms.

OVERVIEW

Initial effort supported by the contract was mainly devoted to obtaining and preparing samples of Westerly granite for experiments. Preliminary experiments to characterize the properties of Westerly granite were performed on small samples obtained from the Bonner Monument Company. Material properties measured agreed well with previous determinations.

A coordination meeting was held with S-Cubed, SRI, DNA, and DARPA representatives on February 1, 1984. During this meeting SRI described initial dynamic tests using Westerly granite. These tests indicated that the electromagnetic properties of Westerly granite made it less suitable for experiments than Sierra White granite in which SRI had performed some exploratory testing. At this meeting the decision was made to shift the dynamic experiments to Sierra White granite. Given this decision the quasi-static experimental program

was shifted to an initial characterization of the properties of Sierra white granite. While samples were being obtained, a study was begun of the failure process in Westerly granite under simulated shock loading. Although electromagnetic interference hindered particle velocity measurements in dynamic experiments with Westerly granite, it remains a suitable material for quasi-static experiments because of the large body of literature documenting its properties. The major questions studied were 1) how would the granite fail, and 2) would the presence of water saturating the rock affect its strength.

Procedures and results obtained in various experiments are described in detail in the following sections. Briefly, the measured elastic properties and density and porosity of Westerly granite agreed well with literature values. The strength of Westerly granite was measured under simulated shock loading and in standard triaxial failure tests. The differences in loading path between the two types of experiments had little, if any, effect on the strength of the rock. Failure occurred in simulated shock loading when the loading path intersected the failure envelope determined by standard triaxial failure tests. Dilatancy was observed during quasi-static unloading from the simulated shock loading. The failure process in low porosity rock appears to be similar to that of standard triaxial tests. Tensile microcracks open causing a relative volume increase and then link to form a weak zone which subsequently fails in shear. Deformation during passage of a shock wave should be undrained. Dilatancy hardening is expected to minimize the effect of pore fluids at reducing the effective stress in rock.

Samples of intact and thermally fractured Sierra White Granite were obtained from SRI. A series of samples were prepared and tested to measure elastic properties and strength of the granite under different confining pressures. These results are described in a later section and summarized in Table 3.

EXPERIMENTAL RESULTS - WESTERLY GRANITE

Contact was made with the Bonner Monument Company at the initiation of the contract to obtain samples of Westerly granite for experiments. Westerly was chosen for testing because of the extensive rock mechanics literature describing its properties. Small samples of granite from the quarry were obtained for initial testing.

Sample preparation. Cubes of Westerly granite received from the quarry were drilled along three orthogonal axes to obtain 1.375 inch diameter cores for triaxial testing. These raw cores were sent to MIT for surface preparation. This involved grinding to a uniform diameter and grinding the sample ends parallel to obtain uniform length right angular cylinders.

Initial tests. Unoriented samples of granite from the Bonner quarry were obtained for preliminary testing. Granite cubes 31.7 mm on a side were cut and the faces ground parallel. The density as received was 2.648 gm/cc. Porosity was measured by comparing dry and saturated sample weights. A cube was dried in a moderate vacuum (=25 inches mercury) at 42°C for 90 hours and periodically weighed. The decay in weight loss with time indicated that further drying would not reduce sample weight significantly. The sample was then immersed in water for one week and re-weighed. The weight difference indicated a minimum porosity of .47%. Both density and porosity are in good agreement with other determinations (e.g., Clark, 1966; Nagy and Florence, 1984).

An aspect of the experimental plan was to separately measure the influence on shock wave propagation of saturation and fracturing. The

extent to which thermal fracturing could increase rock porosity was studied by heating (about 3°C/minute) a 31.8 mm sided cube of Westerly granite for 12 hours at 160°C and then quenching it in cool water. Porosity was then measured by weight change as before. Porosity increased to .56%.

The velocity of compressional waves is sensative to the shape and density of cracks in a rock as well as the degree of saturation. Since waves traverse the entire sample, variations in wave speed may provide a useful way to characterize average changes in saturation of large samples. The velocity of P waves was measured before and after heating the granite cube to establish the magnitude of velocity changes. Piezoelectric transducers (2.25 MHz) were held by a spring loaded jig on opposite faces of the rock cube. One transducer was excited by square waves from a pulse generator and the time of flight measured by the opposite transducer was recorded. A digital oscilloscope with a signal averaging capability was used to record the waveforms. The arrival time was picked as the first visible deviations from a straight line. The waveform analyzed usually represented the average of 50 individual records. Because the wave pulses were very reproducable the signal averaging produced a substantial increase in the signal to noise ratio by reducing the random noise component present on an individual record. Travel times recorded are listed in Table I. The measurements are accurate to about 2%, the uncertainty being dominated by the choice of arrival time. The velocities are about 20% faster than other measurements reported for Westerly granite at room pressure (e.g., Clark, 1966; Heard et al., 1974). Previous room pressure velocity measurements

have scattered more than those at higher pressure, possible due to differing crack populations which close at moderate pressure. By increasing the signal/noise ratio the averaging technique could also be responsible for the faster velocities. An initial velocity anisotropy of 3% was measured between three orthogonal axes. Although marginally resolved considering the uncertainties assigned to the velocity measurements, the anisotropy is real and can be clearly observed in the averaged time records.

P-wave velocities were remeasured after thermal fracturing of the sample. Velocities decreased by about 40% to about 4.3 km/s. The sample was then soaked in water for 24 hours and the velocities remeasured. They recovered to about 5.4 km/s reflecting the absorption of water. Thermal fracturing reduced the velocity anisotropy below the detectable level of about 2%. The reintroduction of water into the sample increased P wave speed by about 25%. Thus, P wave velocities are sensitive to the degree of saturation in the sample.

In summary, tests performed on samples of Westerly granite found values of density and porosity that agreed well with other determinations. P wave velocities measured at room pressure were higher than reported elsewhere (but comparable to values at several hundred bars hydrostatic pressure). The signal averaging technique used here was not used in earlier determinations. Thermal fracturing increased the rock porosity by 20%.

Triaxial fracture tests. Two tests have been performed measuring the fracture strength of room dry right circular cylinders of Westerly granite under standard triaxial loading. The loading path followed in

these tests was to establish a constant confining pressure (σ_3) and then increase the axial stress (σ_1) until failure occurred. Young's modulus E and the shear modulus G were measured during elastic deformation of the sample. These fracture experiments were performed to confirm that deformation of these samples was consistent with previous measurements. The measured fracture strength and elastic constants did agree well with other determinations. Several more tests are planned.

Unconfined strength. One test was performed at room pressure. In all cases the sample was shortened at constant displacement rate in a servo-controlled loading machine. Two sets of strain gages were glued to the sample oriented parallel (ε_1) and perpendicular (ε_3) to its axis. The active element of the wire foil gages was 1.27 cm long. Strains recorded during the experiment are shown in Figure 1. The sample failed at 1.8 kb axial stress (180 Mpa). Compressive strain is considered positive. The figure shows that the sample shortens parallel with its axis and expands radially. Young's modulus $E = \sigma_1/\varepsilon_1$ measured from the initial slope of the parallel strain in Figure 1 is .58 Mb (58 GPa). Figure 2 shows $\varepsilon_1-\varepsilon_3$ plotted against σ_1. The slope of this curve is twice the shear modulus G. The initial slope gives G = .227 Mb (22.7 GPa). These values give a Poisson's ratio at room pressure of .278. Volumetric strain is shown in Figure 3. The sample initially compacts by about .1% as it shortens more than it expands. Then radial expansion accelerates and the sample volume increases as dilatancy occurs. The sample failed at 1.8 kb (180 MPa).

Confined strength. A second fracture test performed at 1 kb (100 MPa) confining pressure is shown in Figures 4 through 6. Parallel and perpendicular strains are shown in the first figure. One parallel gage broke when confining pressure was applied by extruding into a glue bubble or crack. The slight extension seen on the other parallel gage is due to a similar effect. Confining pressure was held constant so these effects were only present at the initial loading. There is a substantial difference in the two ε_3 strains recorded, which probably reflects real dilatancy anisotropy in the rock. Comparable shortening was recorded by both gages when confining pressure was applied. The various elastic parameters calculated from the figures as in the previous experiment are listed in Table 2. These values agree very well with previous measurements (e.g., Heard et al., 1974).

Simulated shock loading. The loading path followed during the passage of a plane shock wave was simulated in quasi-static experiments by loading the sample under uniaxial strain conditions and unloading it by allowing biaxial radial expansion. Uniaxial strain loading of low porosity granite inhibits dilatancy so that the necessary loading path to produce uniaxial strain shows no sign of intersecting the failure envelope at confining pressures of 8 kb (.8 GPa) and differential stresses ($\sigma_1-\sigma_3$) of 13 kb (1.3 GPa; Brace and Riley, 1972).

The difference in loading path between uniaxial stress (standard triaxial failure testing) and simulated shock loading are shown in Figure 7. Here the loading path followed by the two standard fracture tests along with similar failure data from other experiments are plotted in comparison with the loading path followed by a simulated

shock loading experiment. The uniaxial strain loading showed no sign of approaching the triaxially determined failure surface.

The uniaxial strain loading path is determined by requiring no radial strain. The output of two strain gages mounted perpendicular to the cylinder axis were summed and corrected for the effect of pressure on the gages (described in detail later). The summed output was used as feedback to control the confining pressure. An increase in confining pressure inhibits radial expansion of the sample which otherwise would occur as axial load is independently increased. At peak axial stress the sample column was held at fixed length by the servocontrols and the confining pressure was reduced. If ε_1 is zero the unloading path should follow $\sigma_1 = 2\nu\sigma_3$. The slope of the unloading path as confining pressure was reduced agreed with Poisson's ratio measured in other experiments. Sample failure under simulated shock loading occurred when the loading path intersected the failure envelope determined from standard triaxial tests. Thus the differences in loading path between the two types of tests did not affect the strength of the sample.

Strains measured during simulated shock loading are shown in Figure 8. The apparent expansion initially shown by the radial gages (ε_3) is due to the effect of confining pressure on the strain gage output. During unloading at fixed sample column length, the parallel gages continued to shorten by a small amount. This is due to the decreasing modulus of the rock as confining pressure is reduced. Although the overall length of the sample column is constant, the strain partitioning between rock and steel in the sample column changes to concentrate shortening in the rock.

In uniaxial strain $\sigma_1 = (\lambda + 2G)\varepsilon_1$ and $\sigma_3 = \lambda\varepsilon_1$. Figures 8 and 9 show these data and the elastic parameters are listed in Table 2. Poisson's ratio can be calculated either from stress-strain curves or from stress curves alone. Comparison of the independently calculated ratios allows a test of the accuracy of the strain measurements. Given the direct measurement of λ and G from the σ_1 or σ_3 vs. ε_1 curves then $\nu = \lambda/2C\lambda + G)$. Alternatively, in uniaxial strain, $\nu = \sigma_3/(\sigma_1+\sigma_3)$. Poisson's ratio calculated from the stress relation is .30 over the range of σ_3 from 1 to 2 kb. Depending on the parallel gages used, Poisson's ratio calculated from direct measurements of λ and G varied from .29 to .31. The agreement between the two independent techniques is good. The variation in elastic parameters determined by the separate gages probably reflects real anisotropy in the properties of Westerly granite.

Anisotropy is also suggested by comparing the parallel strain vs. differential stress records of uniaxial strain tests UNI2 and UNI3. Parallel gages in test UNI2 were located opposite each other across a diameter of the sample. Similar gages were located with 90° separation on sample UNI3. If deformation is symmetric in the plane of the sample radial cross-sections, then gages with 180° separation should measure similar strain while gages with 90° separations will show more extensive variations. This behavior is shown in Figure 10 when ε_1 (test UNI2) measured at 180° separation tracks well but ε_1 measured at 90° separation (test UNI3) differ noticably.

Sample UNI3 was jacketed and deformed after saturation with the heogene confining medium. Saturation was produced by pressurizing the unjacketed sample to 2 kb (29,000 psi) for about one hour. The

difference in sample weight before and after saturation and the density of kerosene (.82 gm/cc) showed that the volume of kerosene absorbed equalled that expected from a sample with .5% porosity.

Pore fluid is expected to make the sample stiffer, requiring a more rapid increase in confining pressure with increasing axial load to produce uniaxial strain. At confining pressures about 1 kb $d\sigma_3/d\sigma_1$ for sample UNI3 is generally larger than for dry sample UNI2. The variation between samples, however, is sufficiently large to obscure the effect of the kerosene pore fluid. Future experiments will use water as a pore fluid since its properties differ significantly from those of kerosene. Specifically, the viscosity of water is insensitive to pressure up to a kilobar while that of kerosene increases by a factor of 10. Further, the compressibility of kerosene is about a factor of two larger than that of water, so kerosene in pore space has less effect on bulk elastic properties than water.

Pressure effect on strain gages. Wire-foil type resistance strain gages are affected by changes in hydrostatic pressure alone, independent of the strain undergone by the substrate (Brace, 1964). The correction for apparent strain change due to increased hydrostatic pressure alone was calculated by mounting gages on a material with known elastic properties. A rectangular prism of Schott F-2 optical glass (E = 550, 156 bars; σ = .224) was used. Gage output was measured as a function of confining pressure and compared with the strain expected from the known moduli. The calculated strain was systematically larger than the observed strain in agreement with other observations (e.g., Brace, 1964). The strain correction for hydrostatic pressure change was $.34 \cdot 10^{-6}$ bar^{-1} for the Micromeasure-

ments CEA-06-500VW-120 gages used in the experiments with M-Bond AE-15 epoxy. Gages and epoxy from the same manufacturing lots were used in all experiments.

Summary. Samples of Westerly granite have been loaded to failure following two different σ_1, σ_3 loading paths. One path in which confining pressure σ_3 is established and then axial load σ_1 is increased to failure, is standard for triaxial tests. The other path was a quasi-static analog of the loading experienced by rock during the passage of a plane shock wave. Axial load was increased independently of confining pressure. Confining pressure was continually increased at a rate sufficient to produce uniaxial strain deformation. Low porosity rock has never failed in quasistatic uniaxial strain tests. Sample unloading followed a different path. The sample column was kept at fixed length by the servocontrolled loading machine while the confining pressure was reduced. The sample was thus allowed to expand radially. Differential stress increased until the unloading path intersected the failure envelope determined from standard triaxial tests. The different loading paths had no effect on the strength of the low porosity granite. Dilatancy occurred during unloading. The dilatancy hardening effect is expected to reduce the influence of any pore fluid at reducing the effective stress.

Experimental Results - Sierra White Granite

Sample Preparation. Edge pieces from 1 foot dimensional cubes of granite which had had 11 inch diameter cylinders cored out were received from SRI. These cubes are described as "intact" meaning as received from the quarry or "fractured" meaning that the cube had been thermally cycled (at SRI) to induce microfractures. Cylindrical cores 1.375 inches in diameter were cut at Lamont from the samples provided. The smaller cores were parallel to the SRI cores. Sample ends were groud parallel to $\pm$ .001 inches or better. Samples were then jacketed in copper foil which was seated on to the rock by exposing the sealed specimens to 1 kb confining pressure. Micro-measurements strain gages were then glued to the copper foil using micro-measurements AE-I5 epoxy. Samples were cured at 25°C for approximately 12 hours. Fracture tests were then performed on the specimens at different confining pressure to determine the material properties and fracture strength of Sierra White granite as a function of confining pressure. Four strain gags were mounted on each sample and seasoned at 1 kb confining pressure. Gages were oriented parallel with the long cylinder axis, or at right angles to the axis, to measure radial strain. Gages with similar orientation were mounted 90° apart to accentuate strain differences due to anisotropy.

Experiments were performed on dry "fractured" and "intact" samples at confining presures of 10,500.0 and 1,000 bars using the servocontrolled loading machine. Experimental procedure was to establish the confining pressure desired and then begin shortening the samples at a constant displacement rate until failure occurred. A constant shorten-

ing rate of 1 micron/sec was imposed. Elastic constants were determined over a few hundred bar interval in axial load during the initial deformation. The fracture strength was determined by sample failure. Experimental conditions, elastic properties, and failure strength are listed in Table 3.

A set of three graphs is shown for each experiment. Data stop at failure or just afterward. Each set consists of graphs showing the following data. The first figure shows measured radial and axial strain vs. axial stress. The slope of the axial stress vs. axial strain curve is Young's modulus. In all experiments the axial strain is compressive while the radial gages show expansion. The second figure shows volumetric strain, calculated from the sum of the parallel and twice the radial strain, vs. axial stress, σ_1. The samples compress initially as axial load increases and then expand, indicating dilatancy. The final figure in a set shows axial strain minus radial strain vs. axial stress. Under the assumption of liner elasticity one can show that $G = \sigma_1/2(\varepsilon_1-\varepsilon_3)$ where G is the shear modulus. A_1 axial stress is σ_1 and axial and radial strains are ε_1 and ε_3. Shear modulus is calculated from the slope of the final figure in a set.

The general behavior measured during deformation is similar to that of other granites. Features of note in the individual experiments are discussed later. In general the "intact" specimens have slightly higher fracture strength (about 1%) than the "fractured" samples and also are stiffer by a few percent. This behavior is expected since the thermal cycling should introduce cracks into the material which should weaken it and make it more compliant. The room pressure experiments should be used with caution since room pressure experiments traditionally show more scatter than those with confining pressure applied. Comparing

Tables 2 and 3, at the same pressure Sierra White Granite has a lower fracture strength than Westerly Granite but a higher Young's Modulus and a slightly higher shear modulus.

Individual Experiments

The data from experiment SI-1 are typical of all the experiments and of experiments using other granites. Data shown in the initial Figure of the set represent raw transducer output as digitized. Output from two radial and one axial strain gage was recorded. Some initial electronic noise is present, represented by sudden spikes. The initial application of confining pressure is shown by compression (shown as positive strain) on all gages. When the sample is shortened the axial gage continues to compress, but the radial gages begin to expand. The sample is deforming by shortening axially and expanding radially. After about -5000 microstrain on the radial gages the sample has developed major cracks and has essentially failed. Strain is very inhomogeneous and the gages begin to physically fail as connections or the foil elements are disrupted.

Volumetric strain is shown in Figure 2. The sample volume decreases initially as the load on it increases. Eventually new crack formation, leading to a volume increase, overcomes compaction due to increasing load and the sample begins to relatively expand.

The third figure in an experimental set is used to determine the shear modulus. Strain shown in Figure 3 is consistent with the assumption of isotropic deformation. The shear modulus is relatively constant to at least 2500-3000 bars axial stress or about 60% of the failure strength.

Experiments SI-2 and SF-5 were performed at room pressure. Confining pressure is not aiding the glue in maintaining intimate contact between the strain gages and the rock. Also any cracks present in the sample are open, not closed by confining pressure. Both radial and axial gages indicate substantial heterogenity in strain, especially on initial loading. Cracks in the plane normal to the sample axis will be closed by the increasing axial load, producing more uniform properties along the axial direction. The similar behavior of the axial strain gages after the initial axial loading suggests that the initial nonuniform strain is due to a nonisotropic crack distribution, not to variable glue properties. The variation in fracture strength traditionally observed in unconfined experiments also indicates real variations in physical properties not an experimental artifact.

Conclusion

Quasistatic triaxial tests were performed on samples of Sierra White Granite to measure elastic constants and begin to define a failure envelope. Results are summarized in Table 3. Thermal fracturing was used to alter the physical properties of the granite in order to test numerical models. The attempt to alter the physical properties of Sierra White Granite by thermal fracturing was detectable in the quasistatic measurements, but did not result in large changes. Heating to a higher temperature is recommended to produce more damage.

Deformation of Westerly Granite was measured under standard triaxial loading conditions and under a loading path mimicing shock wave passage. Unlike high porosity rocks, the different loading paths did

not substantially affect the strength of the low porosity granite. The failure envelope determined in standard triaxial tests agreed well with that measured under simulated shock loading.

REFERENCES

Brace, W., Effect of pressure on electric resistance strain gages, Experi. Mech., 4, 2212-216, 1964.

Brace, W., and D. Riley, Static uniaxial deformation of 15 rocks to 30 kb, Int. Rock Mech. Min. Sci., 9, 271-288, 1972.

Clark, S.P. editor, Handbook of Physical Constants, Mem. 97, Geol. Soc. Am., 1966.

Heard, H., A. Abey, B. Bonner, and R. Schock, Mechanical behavior of dry Westerly Granite at high pressure, Lawrence Livermore Lab, UCRL-51642, 1974.

Nagy, G., and A. Florence, Spherical wave propagation in rocks, Bimonthly Progress Rept No. 4, 23 Dec. 1983 to 23 Feb. 1984, 1984.

TABLE I

Compressional Wave Velocity of Intact and Fractured Westerly Granite

	Length cm	Travel Time microsec	Velocity km/s
As Received			
X	3.178	5.25±.1	6.05±.1
Y	3.180	5.2	6.12
Z	3.178	5.35	5.94
	Travel times are corrected by -.2μs to account for transducer bonding delays.		
Fractured, Dry			
X		7.34±.1	4.33±.1
Y		7.59	4.21
Z		7.59	4.21
	Bonding delay correction -.16μs.		
Fractured, Wet			
X		5.88±.1	5.40±.1
Y		5.88	5.41
Z		5.98	5.31
	Bonding delay correction -.12μs		

TABLE II

Westerly Granite Elastic Constants and Strength

Test	Young's Modulus Mb	Shear Modulus Mb	Poisson's Ratio	Test Conditions
WGB0	.58	.227	.28	Confining pressure 1 bar, peak strength 1.8 kb. Moduli determined from 0-1 kb, σ_1.
WGB1	.65	.258	.26	Confining pressure 1 kb. Peak strength 8.3 kb. Moduli determined from 1-4 kb σ_1.
WGUNI2	.77	.299	.28	Simulated shock loading. Moduli deterimined in uniaxial strain from 1-2.5 kb σ_3. Sample failed during biaxial unloading at σ_1 = 5827 b, σ_3 = 367 b.
WGUNI3	.73-.68	.28-.26	.30	Simulated shock loading, kerosene saturated. Moduli determined in uniaxial strain from 1-2.5 kb σ_3. Sample failed during biaxial unloading at σ_1 = 5648 b, σ_3 = 455 b.

Table III

Experiment	Pc_1b bars	E_4 Megabars	G Mb.	V	Fracture strength, σ_1 bars
SI1	507	.65	.26	.25	5687
SI2	1	.51			
		.58	.18		1598
SI3	1001	.73	.27	.35	7991
SF4	501	.65	.26	.25	5614
SF5	1	.49	.18	.36	1661
SF6	1004	.71	.28	.27	7932

SI denotes "intact sample"

SF denotes "fractured sample"

All samples deformed dry, as received.

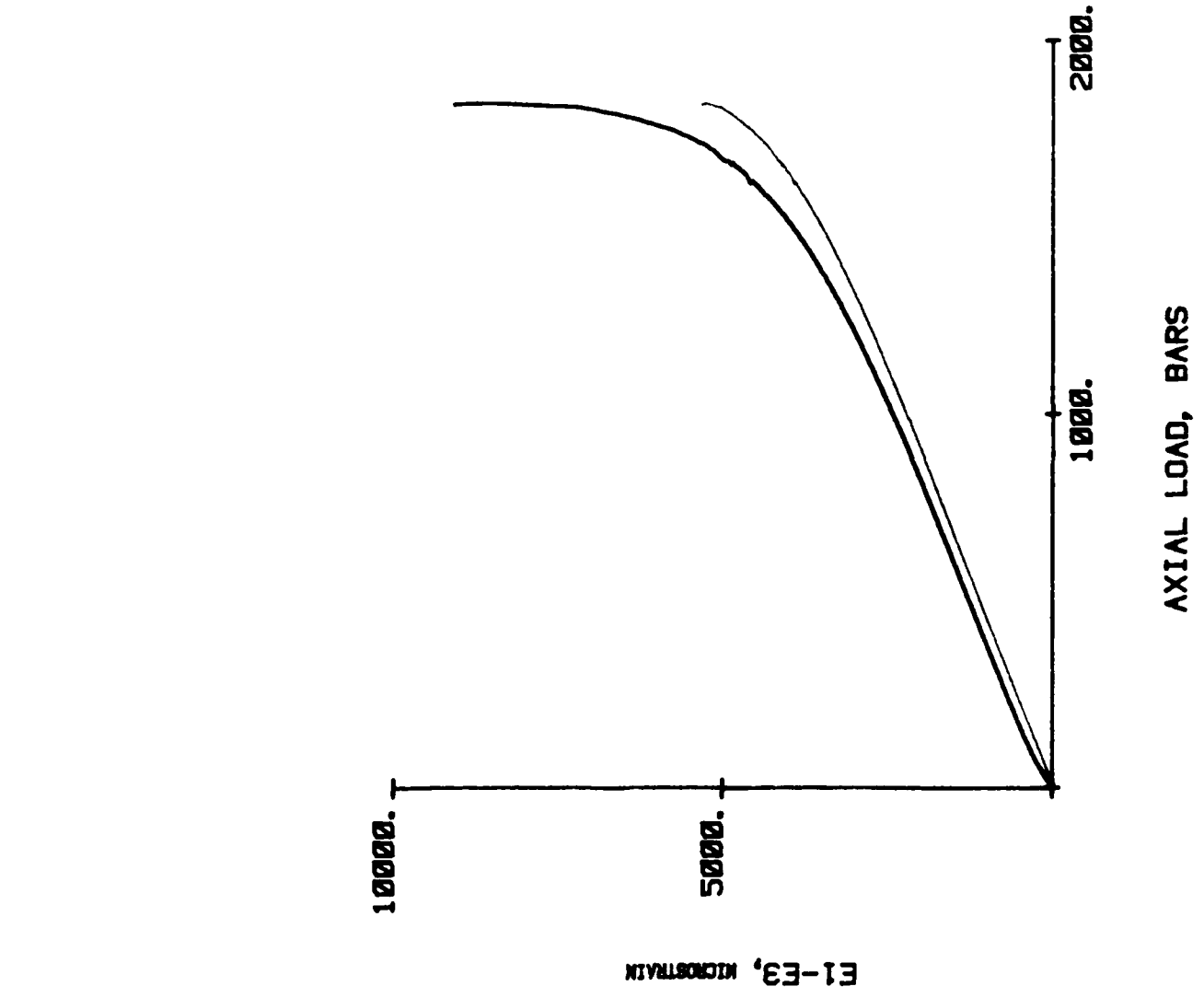
TEST WGB0
E1-E3, MICROSTRAIN
10000.
5000.
AXIAL LOAD, BARS
2000.
1000.

FIGURE ONE

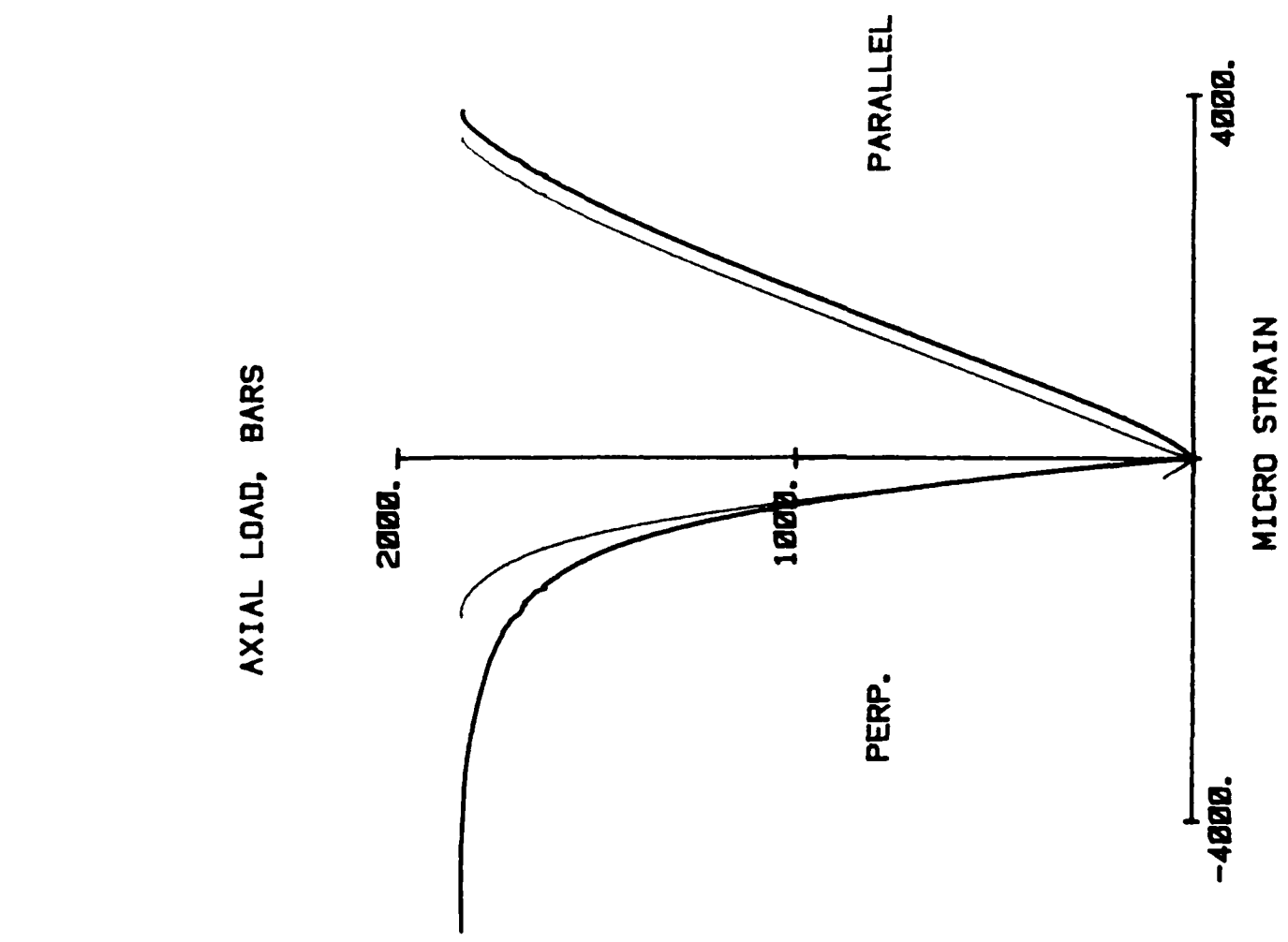
TEST WGB0
AXIAL LOAD, BARS
2000.
1000.
PERP.
PARALLEL
4000.
-4000.
MICRO STRAIN

FIGURE TWO

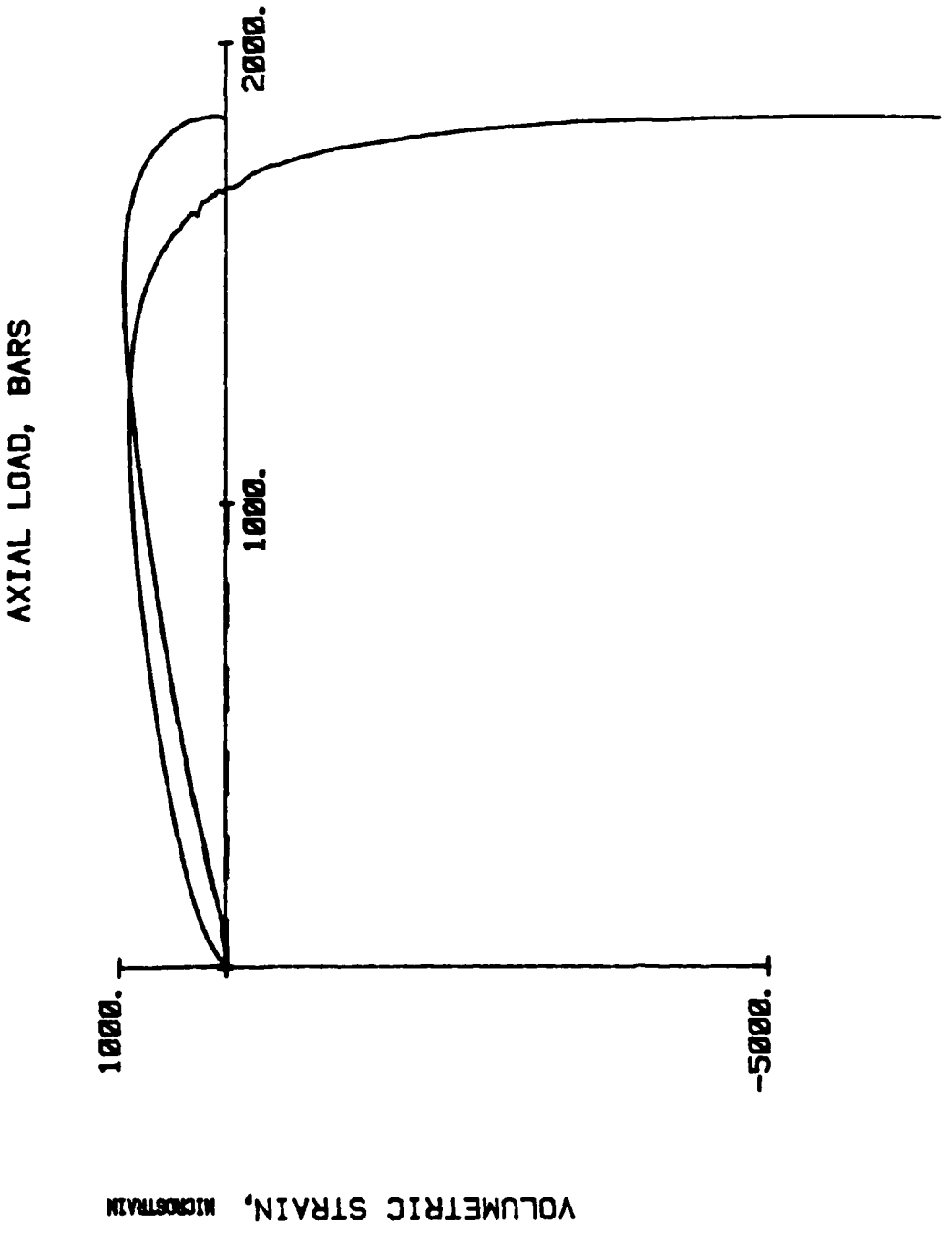

FIGURE THREE

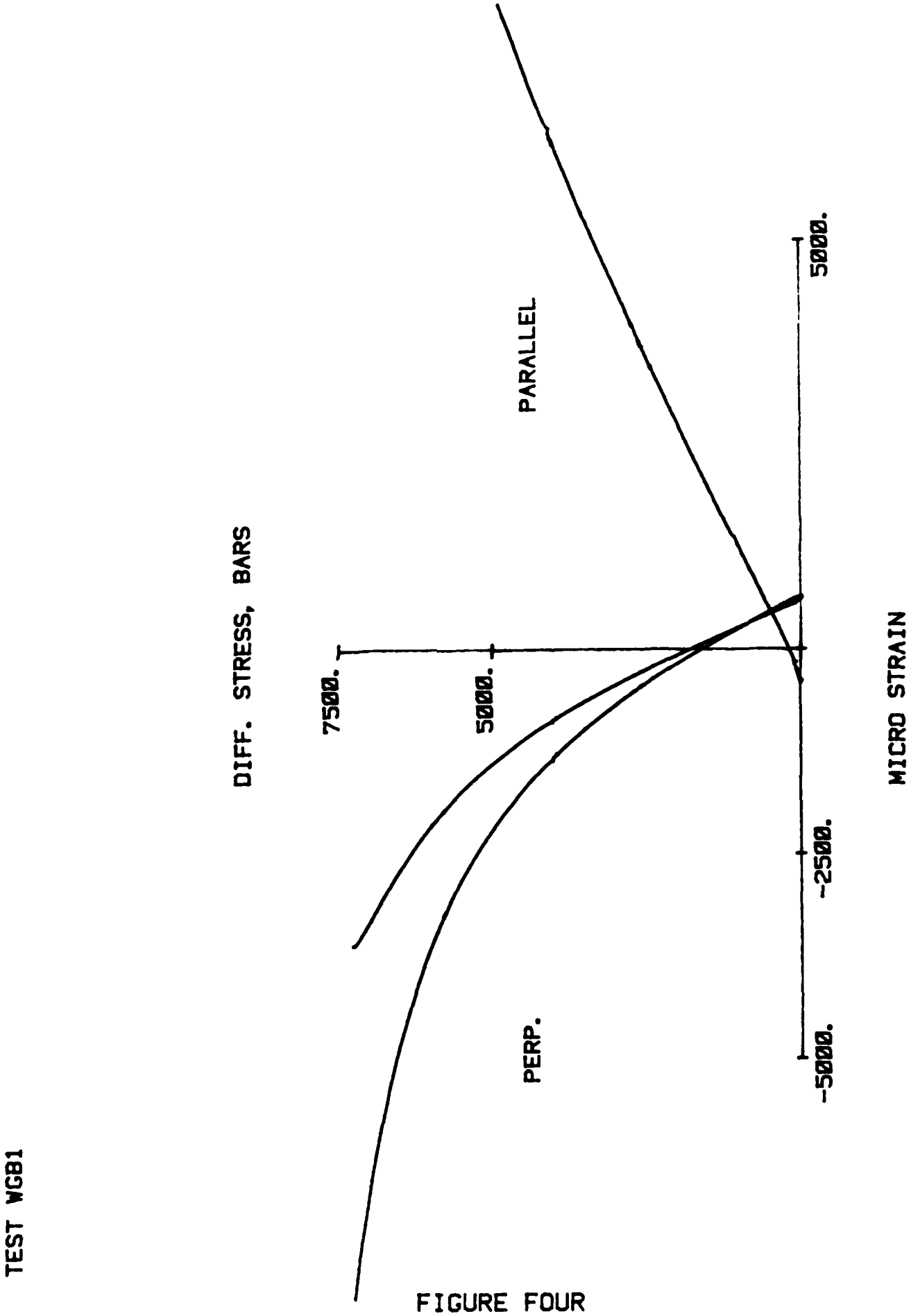
TEST WGB1
DIFF. STRESS, BARS
7500.
5000.
PARALLEL
PERP.
5000.
-2500.
-5000.
MICRO STRAIN

FIGURE FOUR

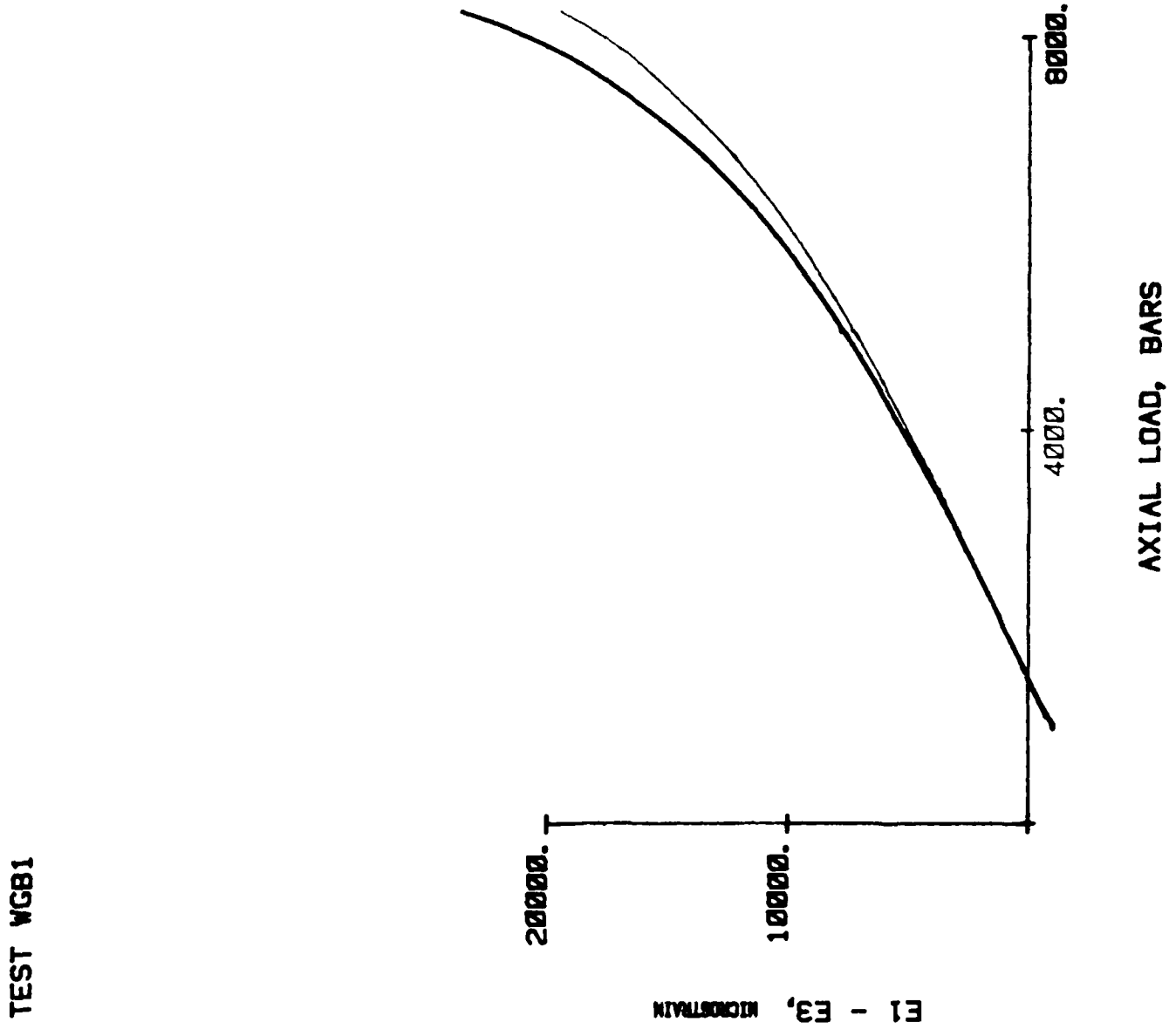
TEST WGB1
20000.
10000.
E1 - E3, MICROSTRAIN
8000.
4000.
AXIAL LOAD, BARS

FIGURE FIVE

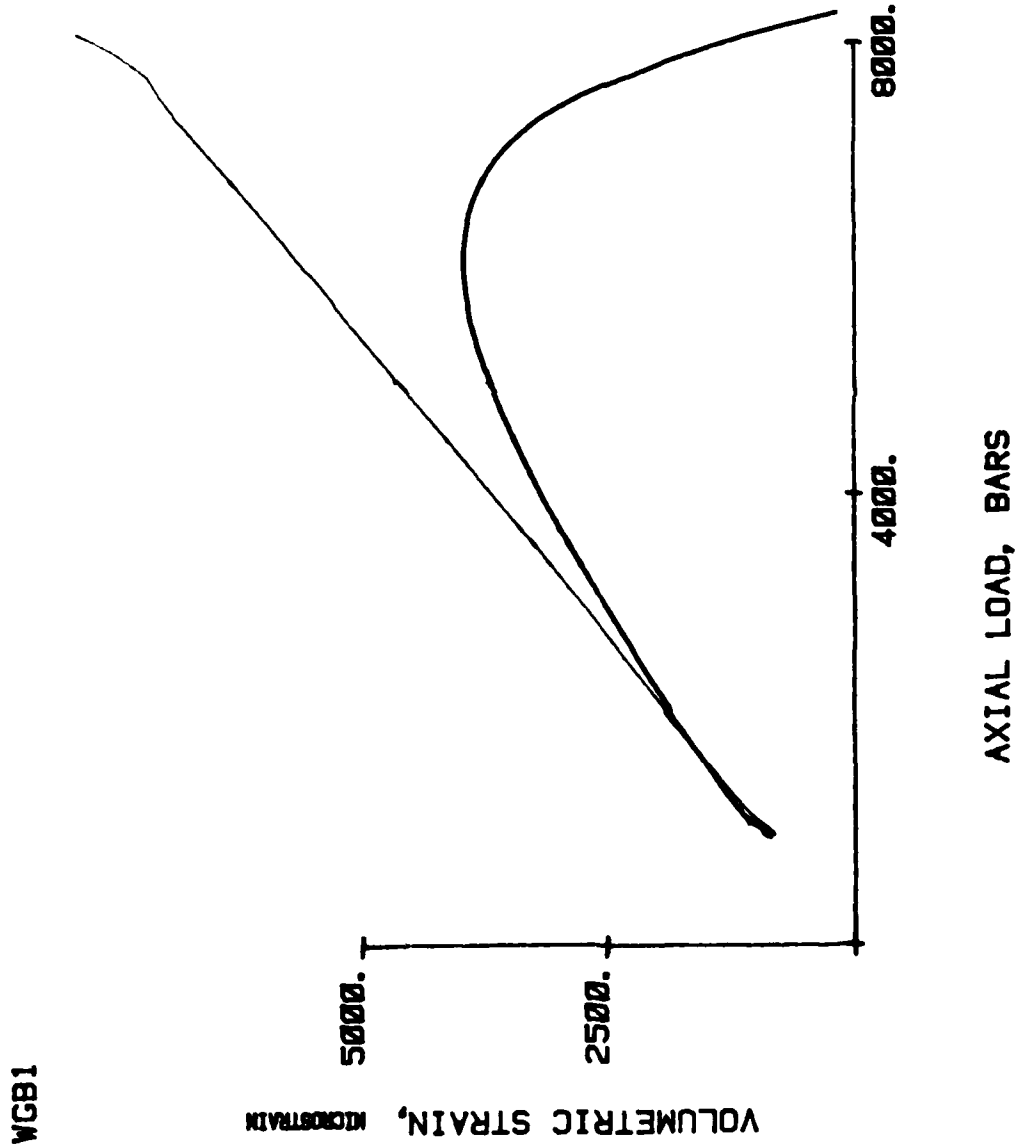
TEST WGB1
VOLUMETRIC STRAIN, MICROSTRAIN
5000.
2500.
4000.
8000.
AXIAL LOAD, BARS

FIGURE SIX

FIGURE SEVEN

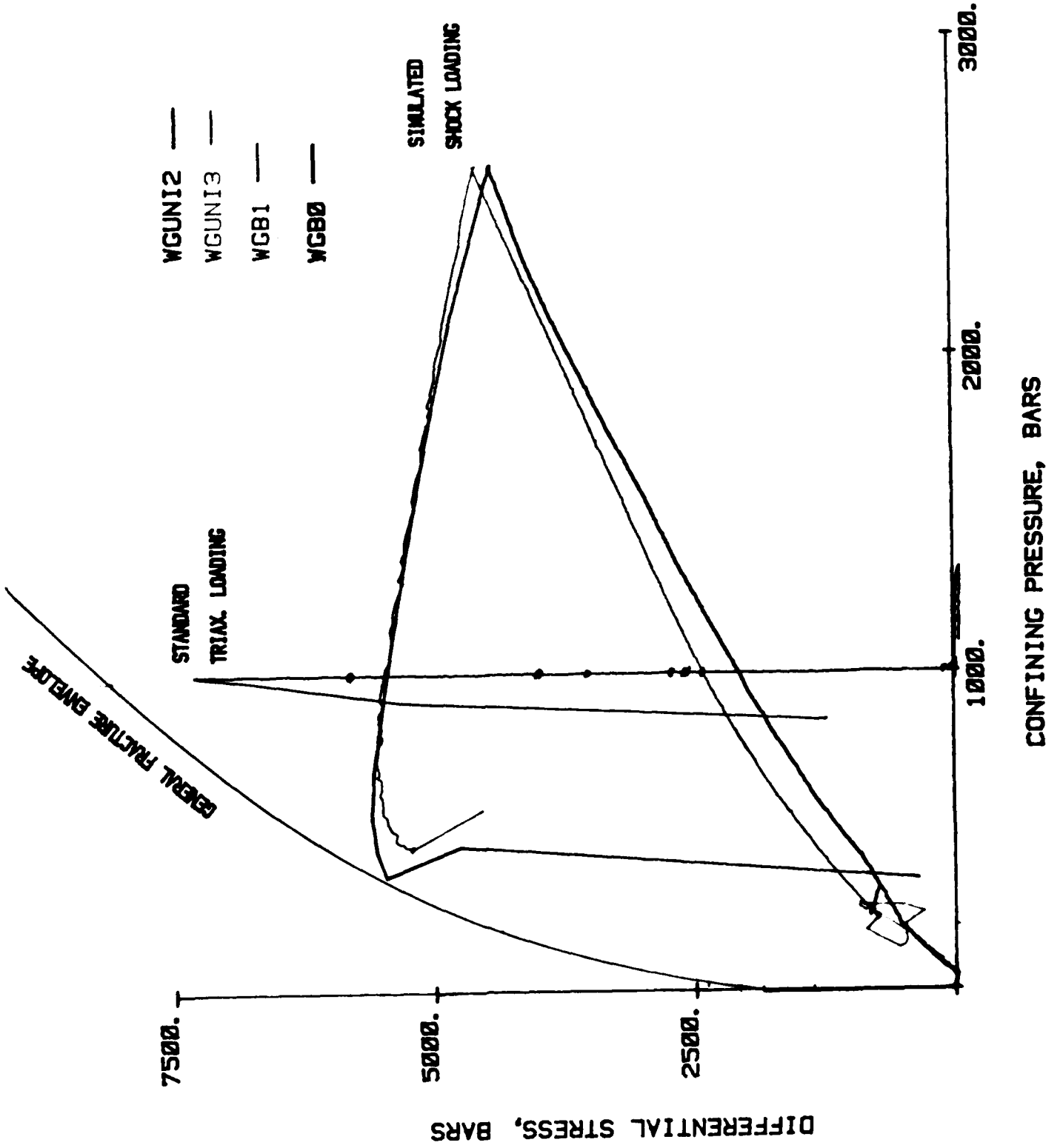

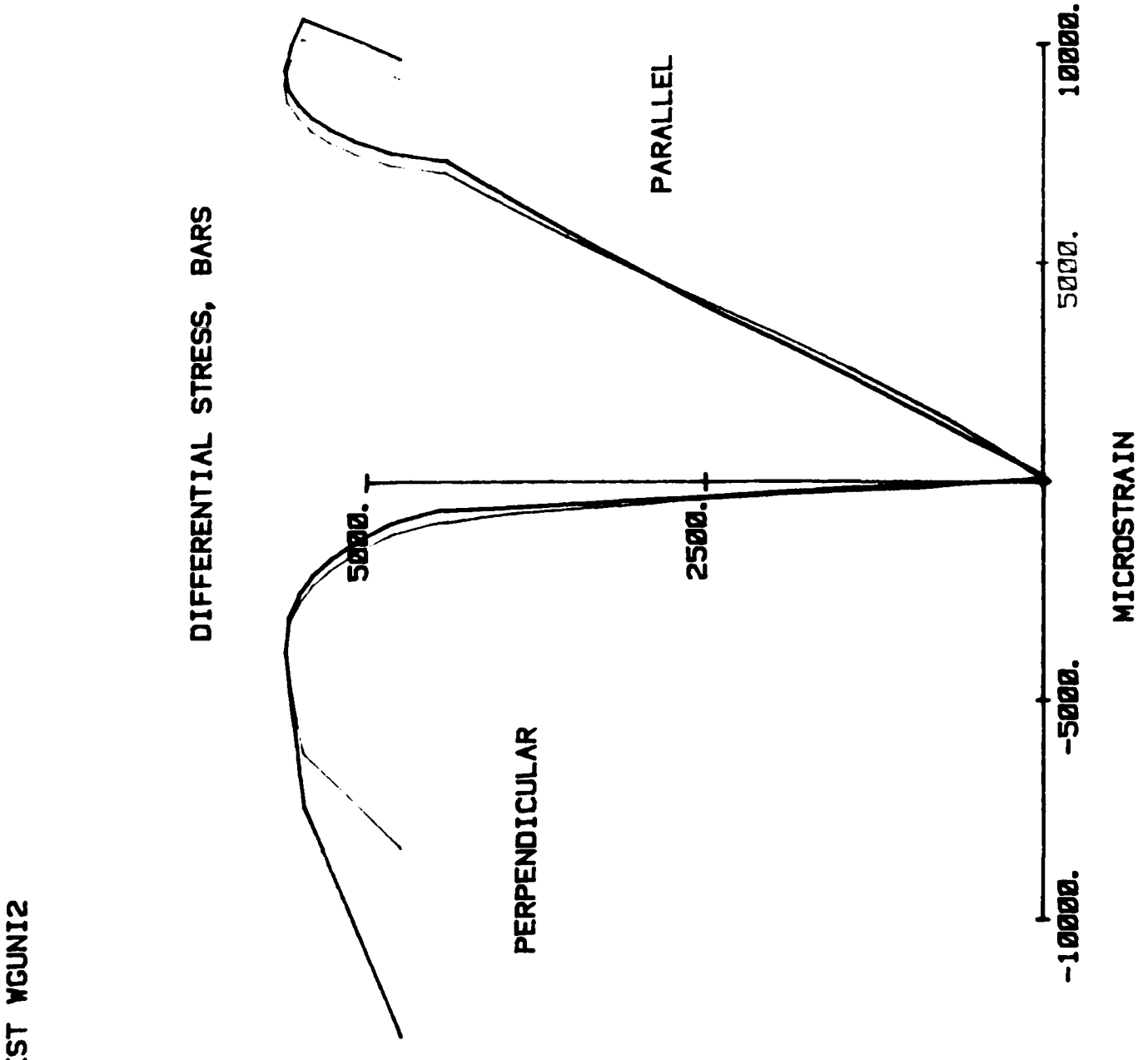

FIGURE EIGHT

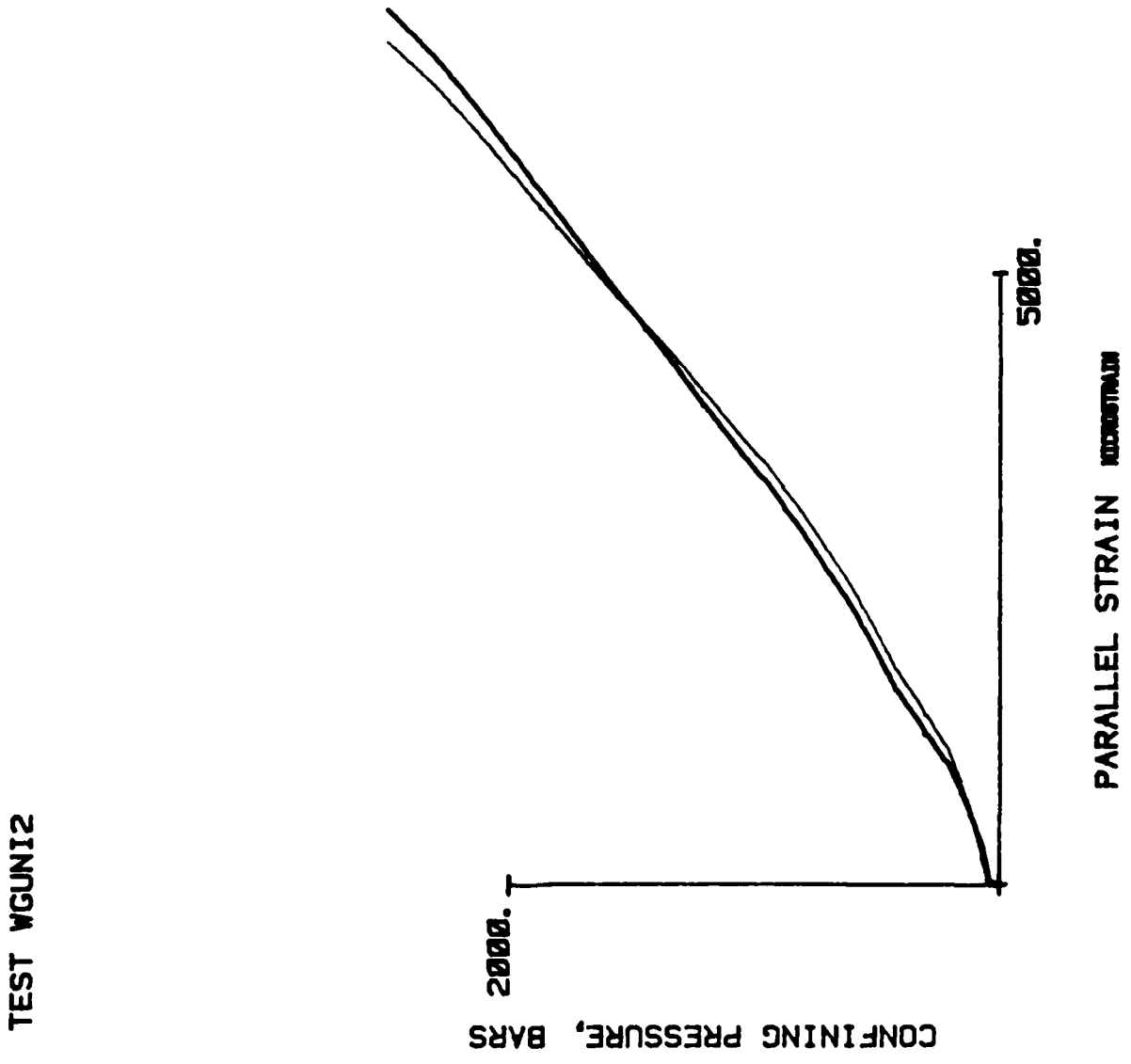
TEST WGUN12
CONFINING PRESSURE, BARS
2000.
5000.
PARALLEL STRAIN

FIGURE NINE

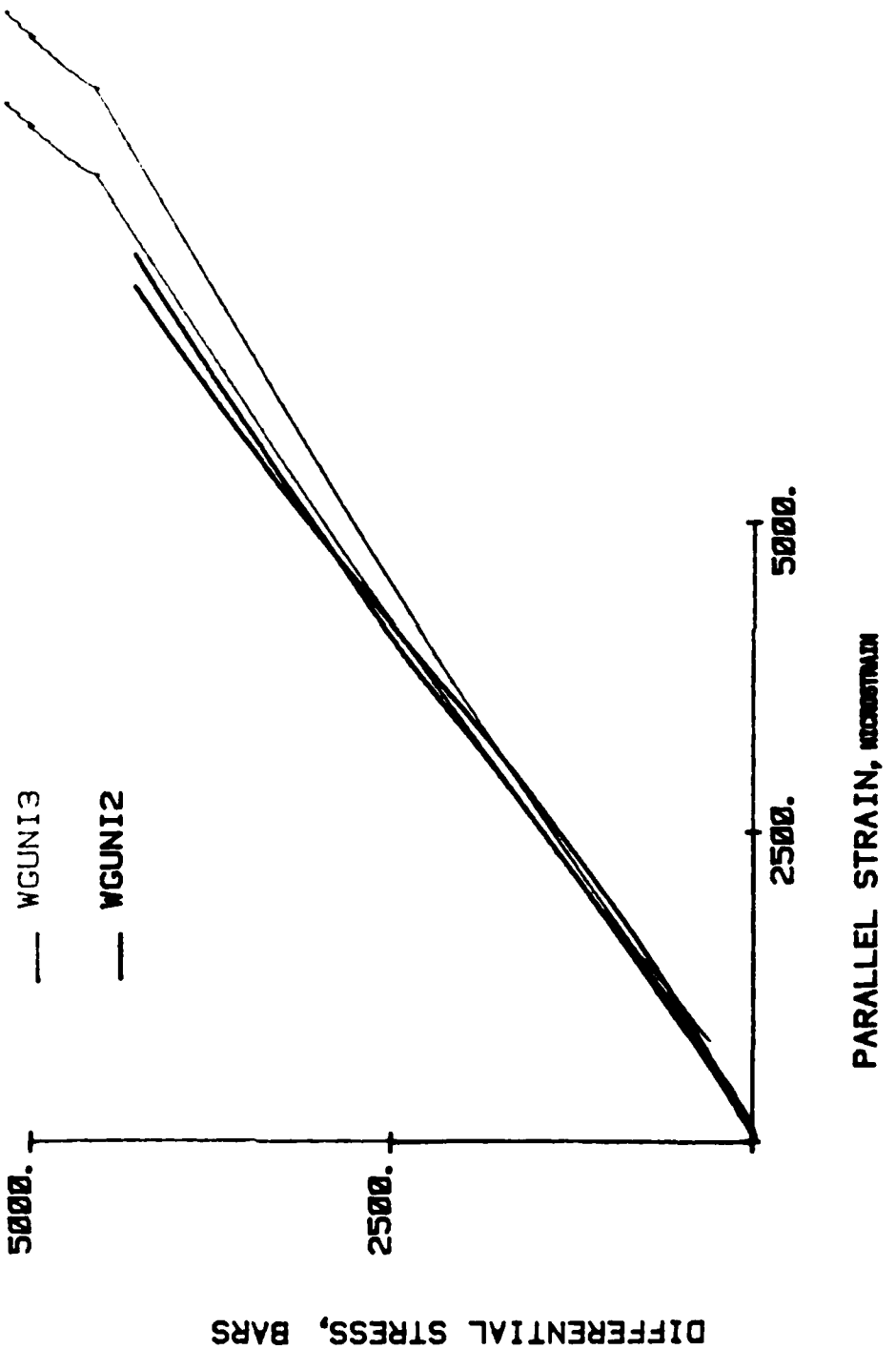
WGUNI3
WGUNI2
5000.
2500.
DIFFERENTIAL STRESS, BARS
5000.
2500.
PARALLEL STRAIN,

FIGURE TEN

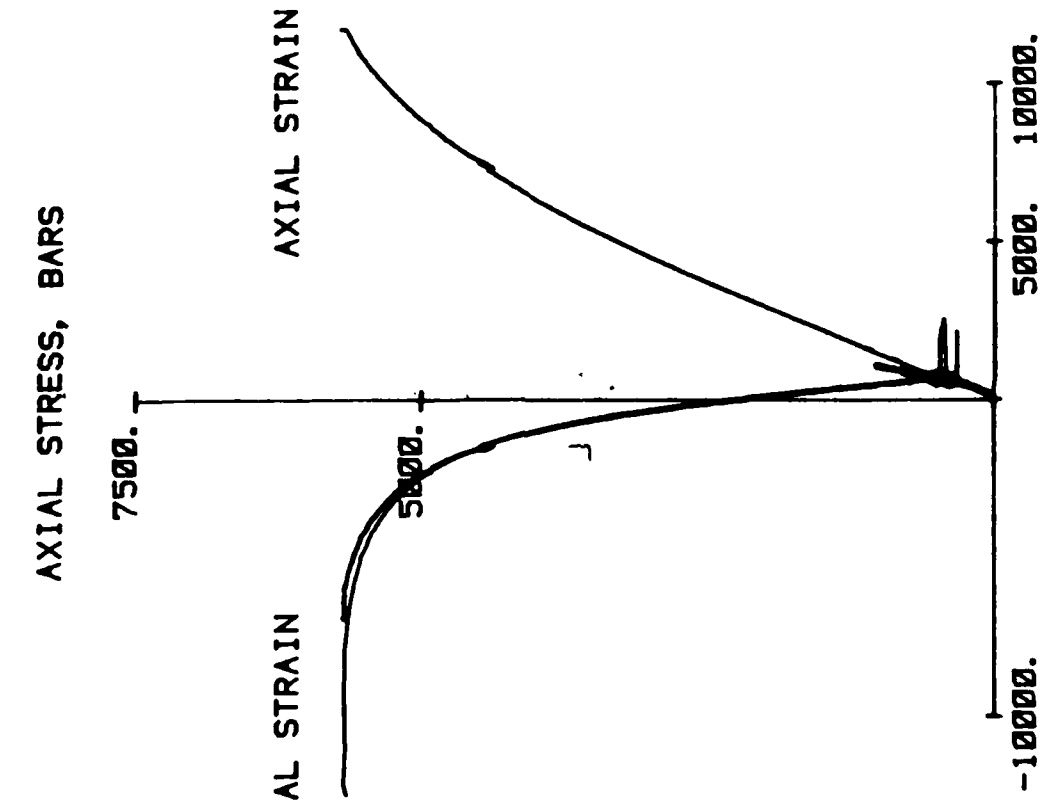
EXPERIMENT SI_1
AXIAL STRESS, BARS
7500.
5000.
AXIAL STRAIN
RADIAL STRAIN
5000.
10000.
-10000.
STRAIN X 10**6

Figure 11

EXPERIMENT SI_1

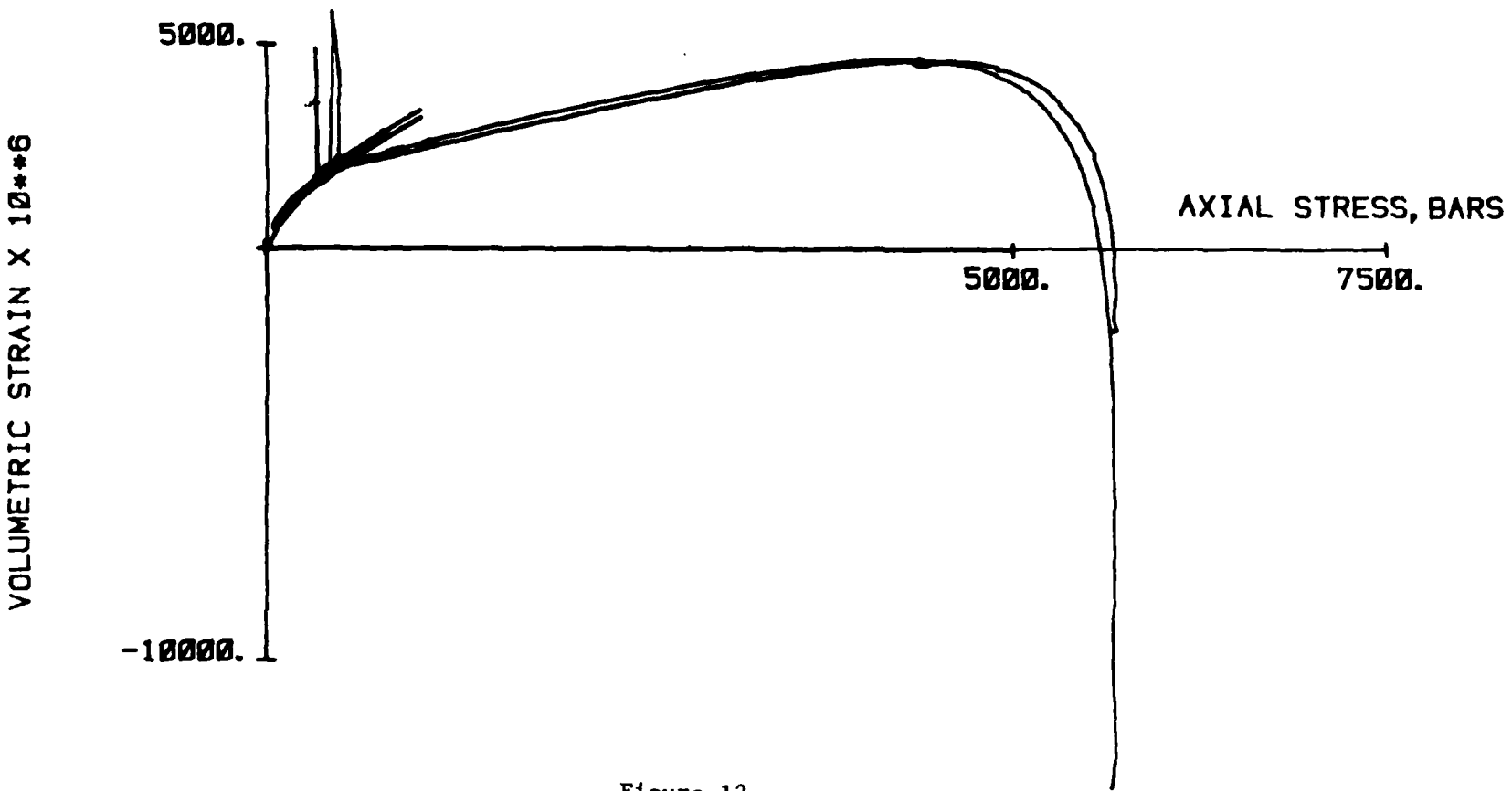

Figure 12

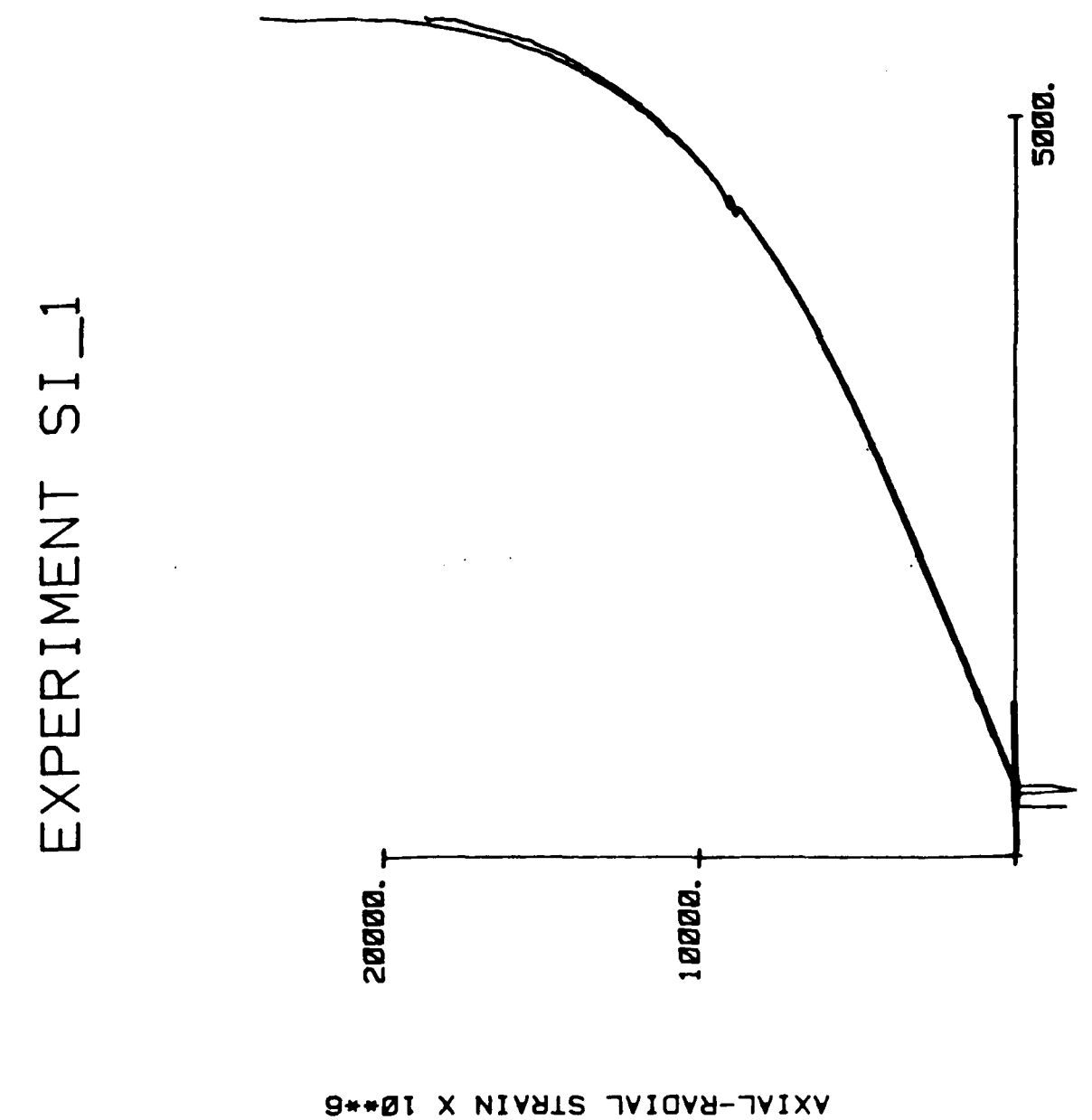
EXPERIMENT SI_1
AXIAL-RADIAL STRAIN X 10**6
20000.
10000.
5000.
AXIAL STRESS, BARS

Figure 13

EXPERIMENT SI_2

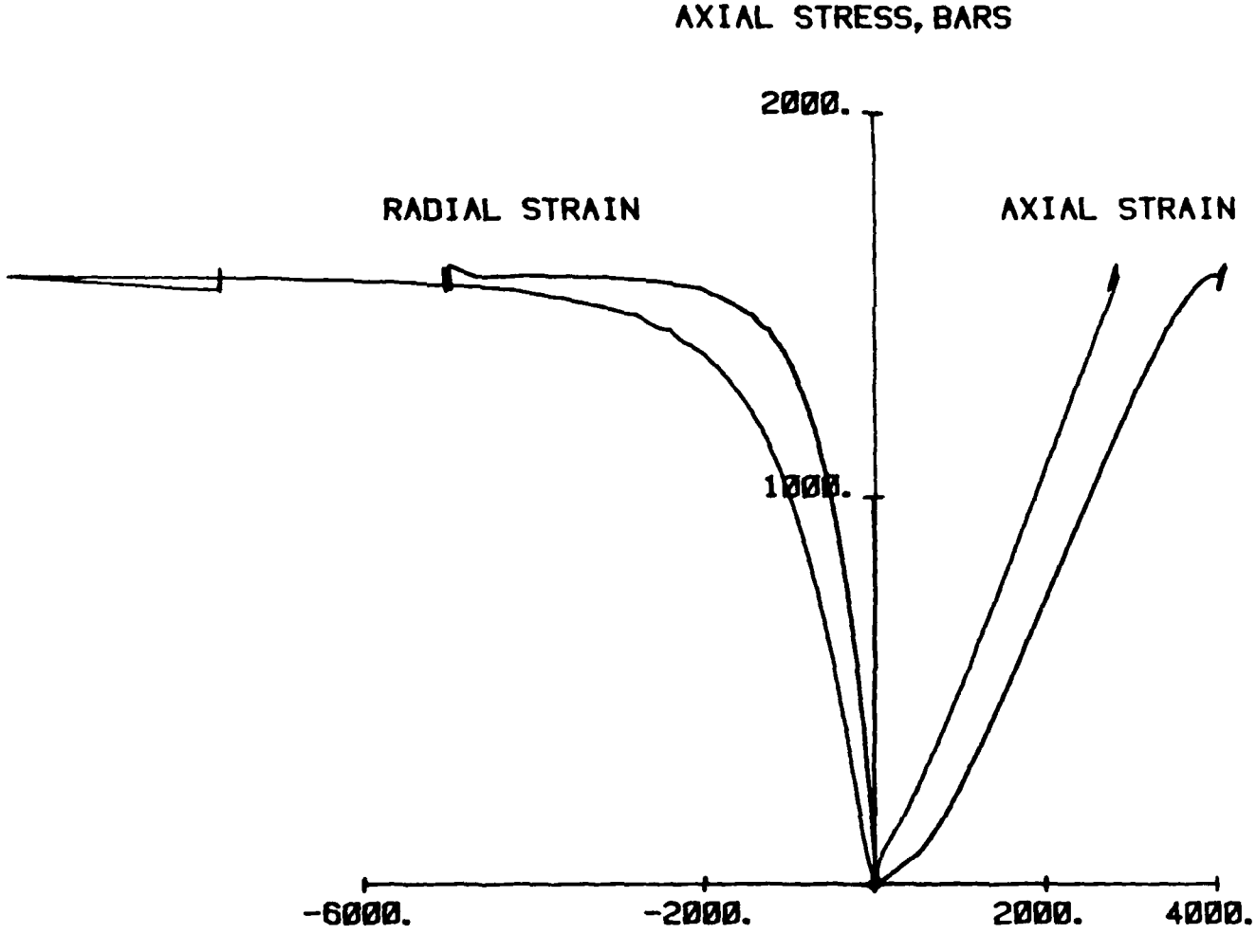

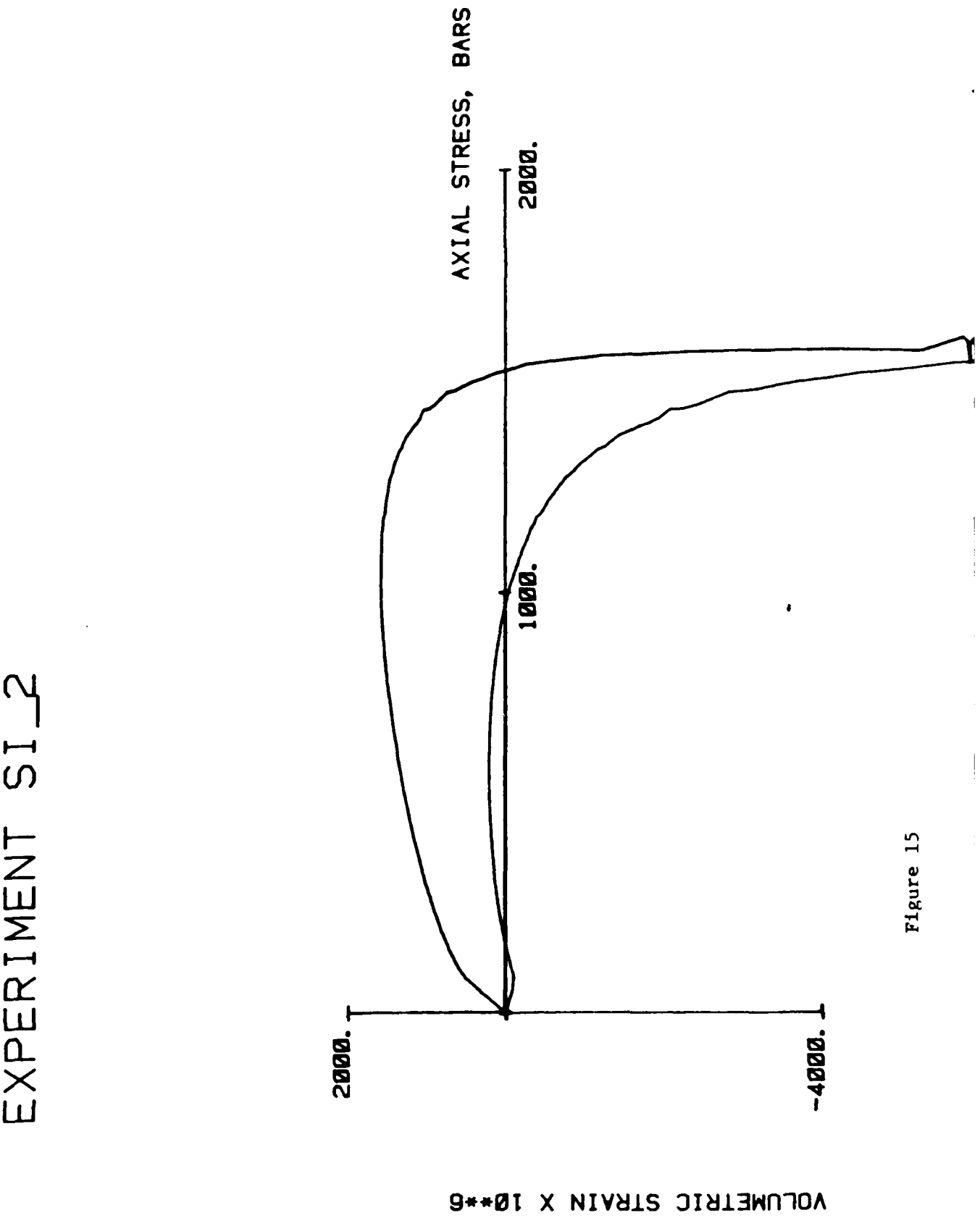
EXPERIMENT SI_2
AXIAL STRESS, BARS
2000.
1000.
2000.
-4000.
VOLUMETRIC STRAIN X 10**6

Figure 15

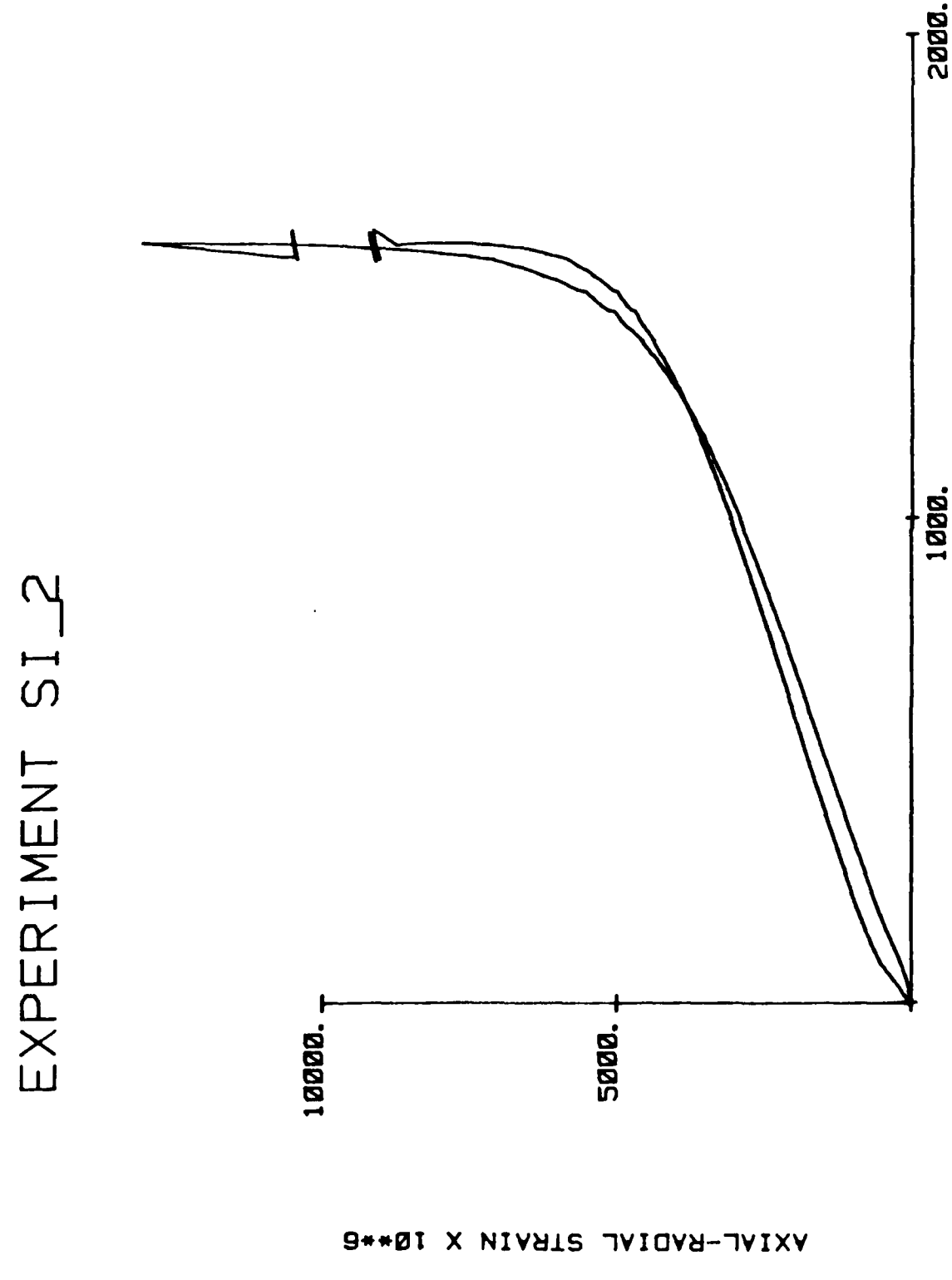
EXPERIMENT SI_2
10000.
5000.
0.
1000.
2000.
AXIAL STRESS, BARS
AXIAL-RADIAL STRAIN X 10**6

Figure 16

EXPERIMENT SI_3

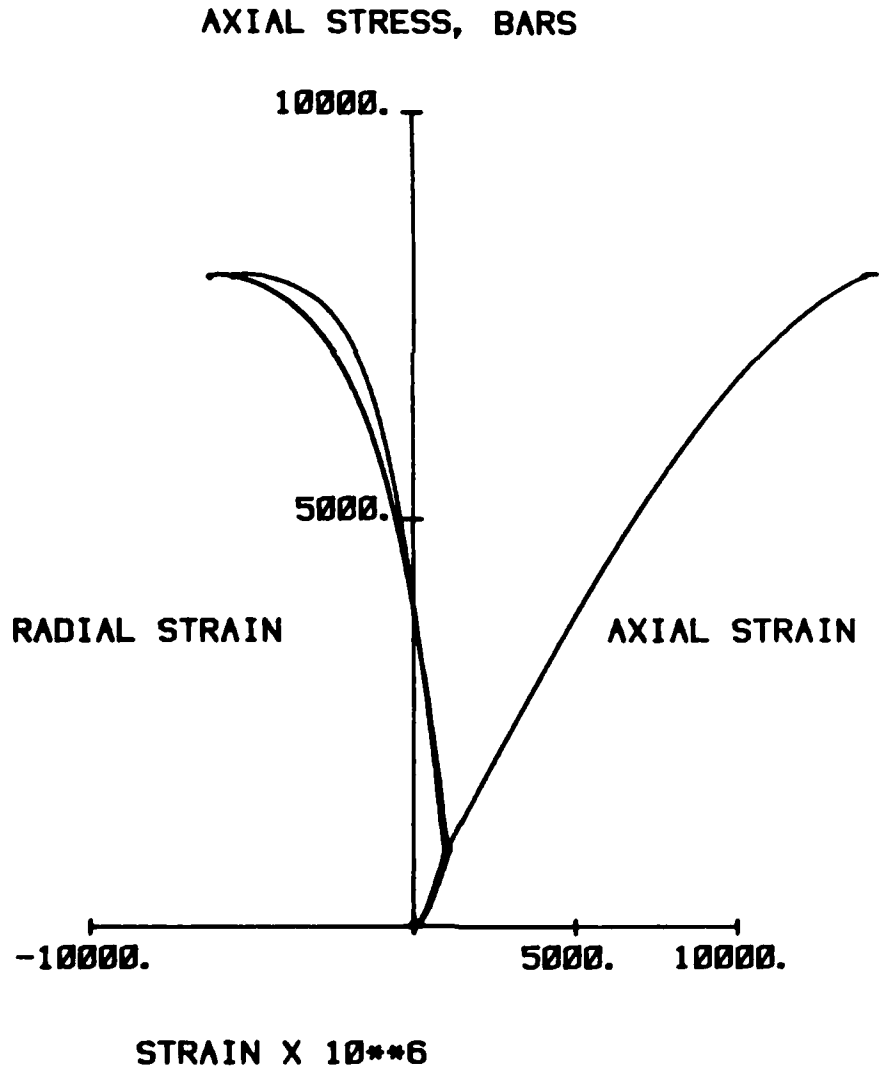

Figure 17

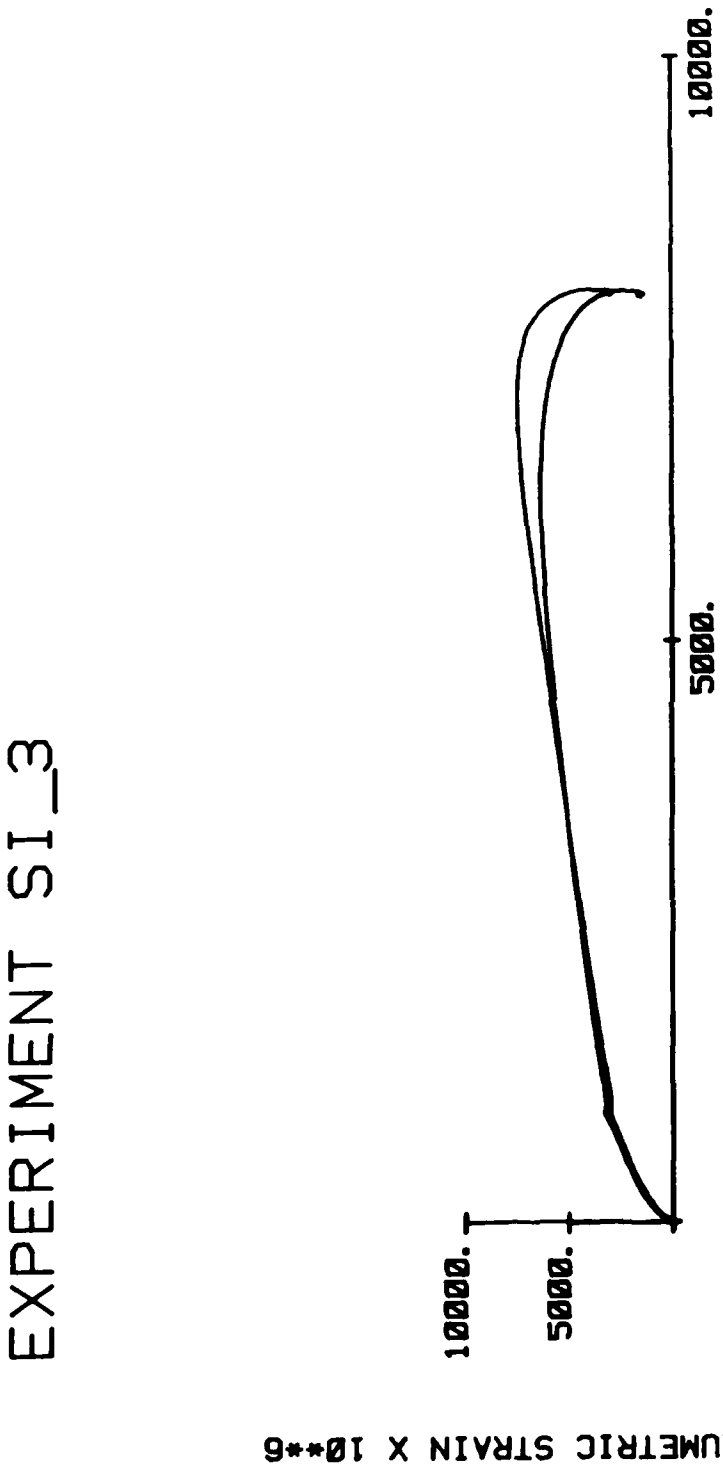
EXPERIMENT SI_3
10000.
5000.
VOLUMETRIC STRAIN X 10**6
10000.
5000.
AXIAL STRESS, BARS

Figure 18

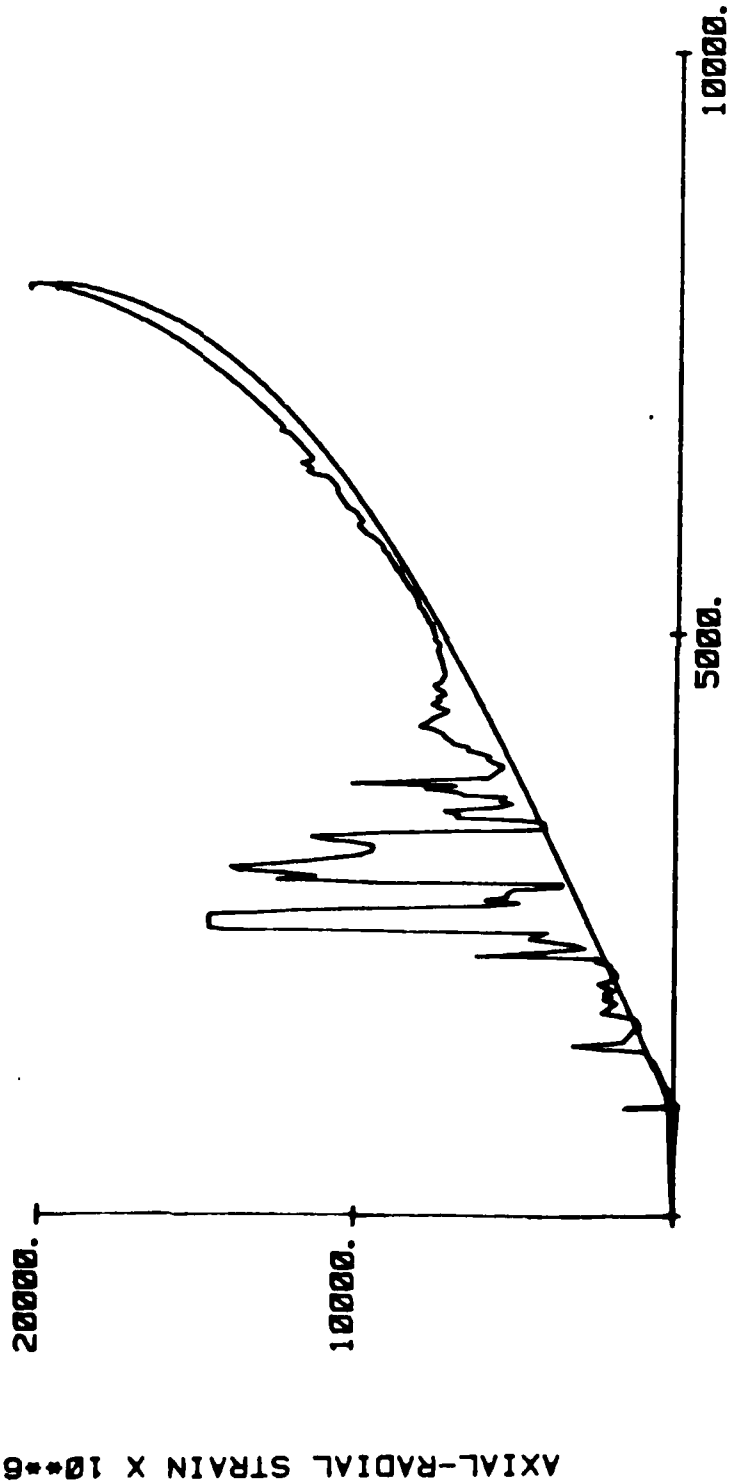
EXPERIMENT SI_3
AXIAL-RADIAL STRAIN X 10**6
20000.
10000.
5000.
10000.
AXIAL STRESS, BARS

Figure 19

EXPERIMENT SF_4

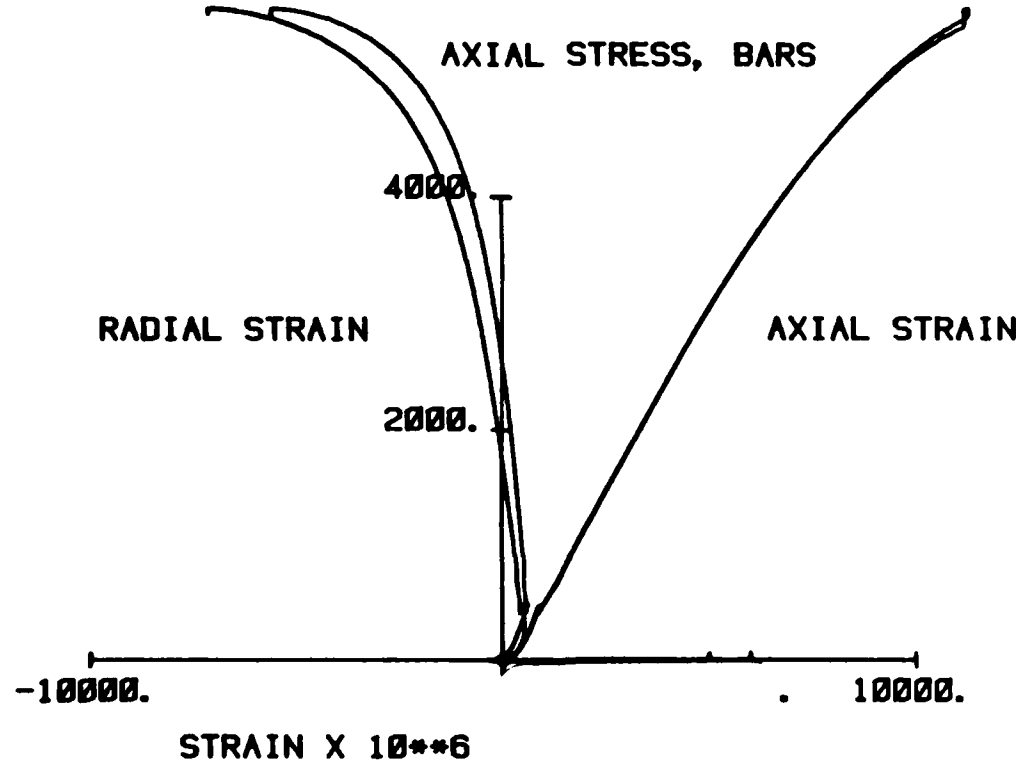

Figure 20

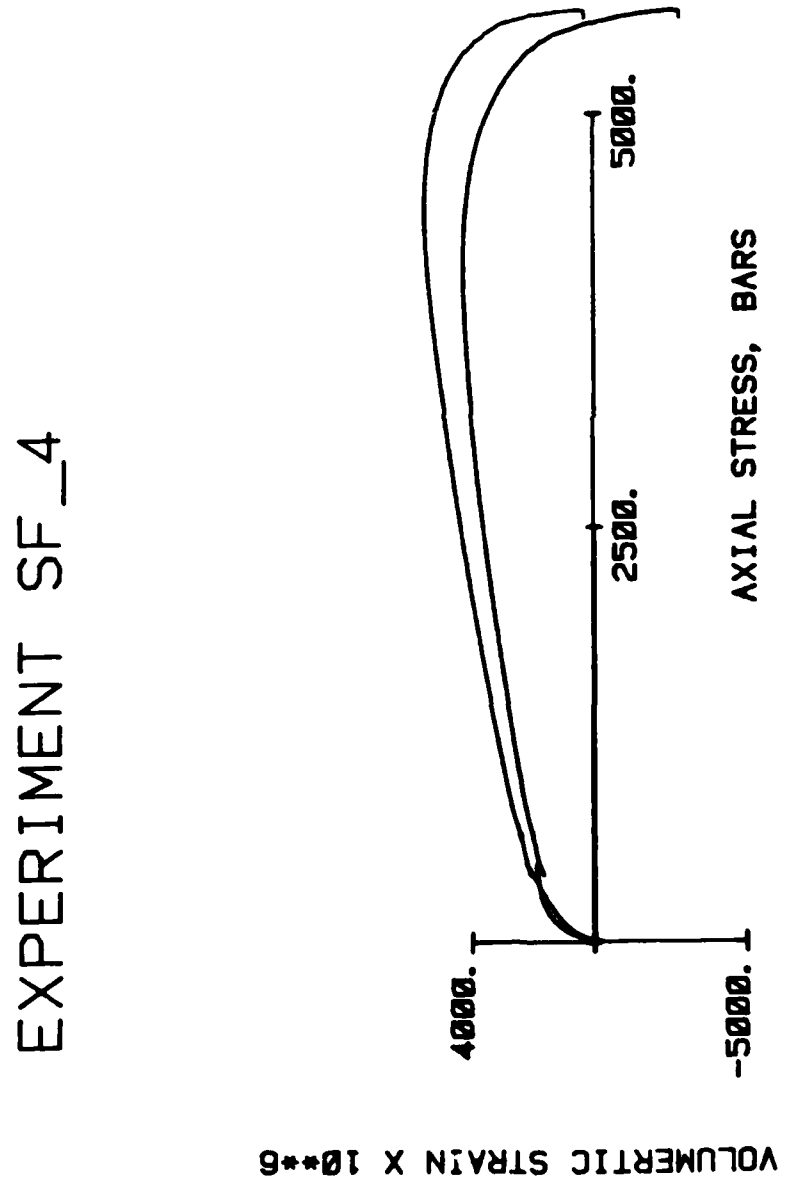
EXPERIMENT SF_4
5000.
2500.
AXIAL STRESS, BARS
4000.
-5000.
VOLUMERTIC STRAIN X 10**6

Figure 21

EXPERIMENT SF_4

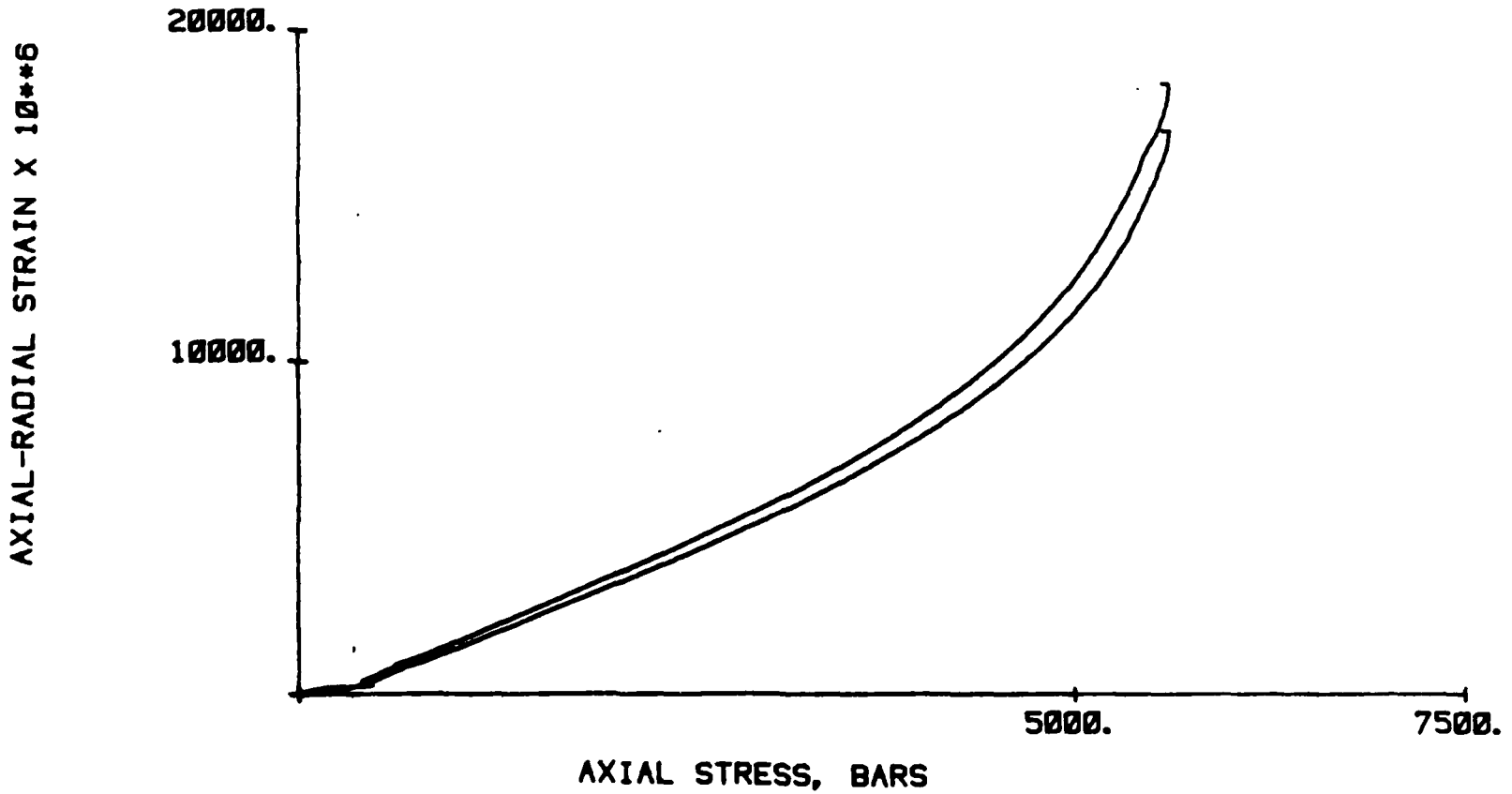

Figure 22

EXPERIMENT SF_5

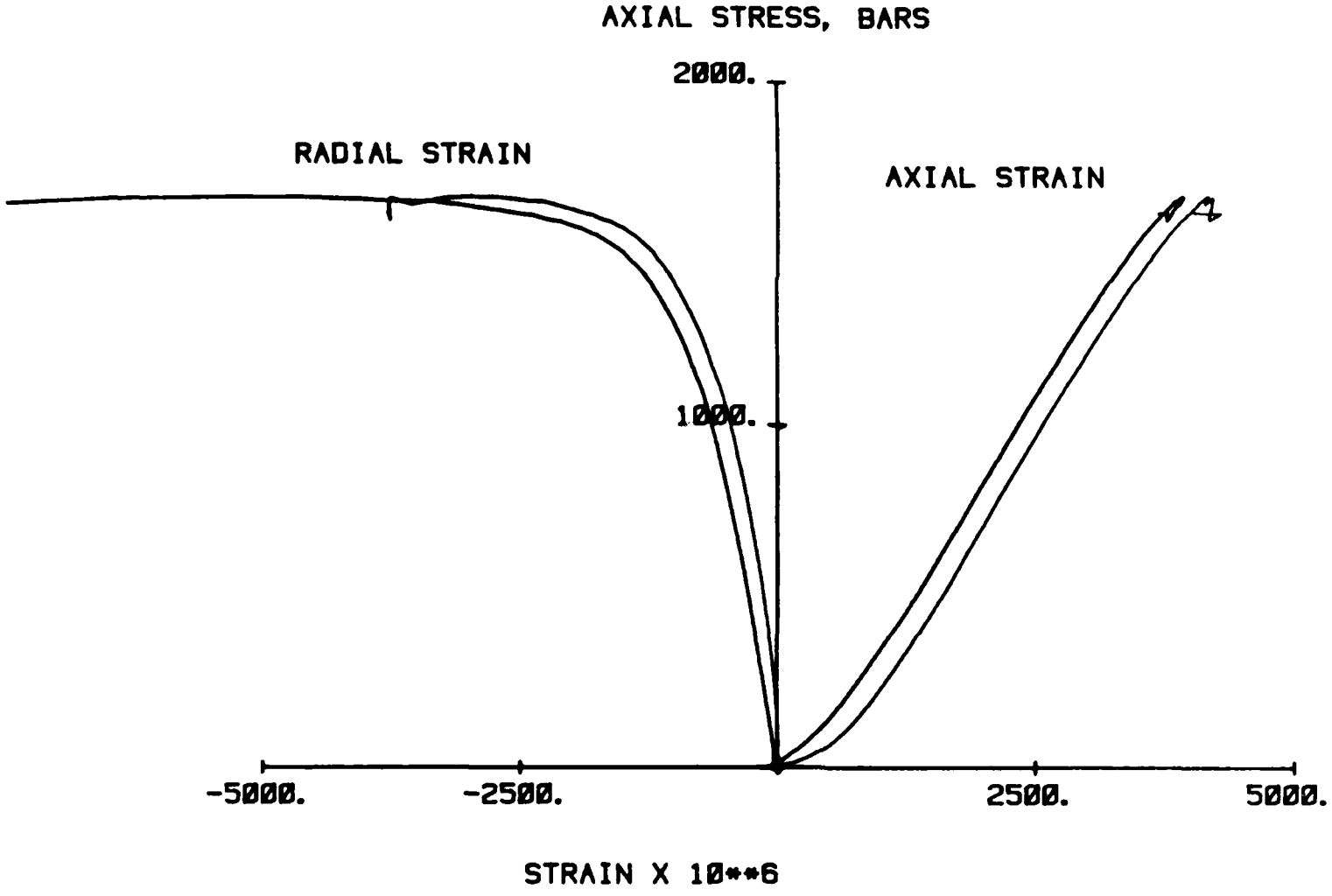

Figure 23

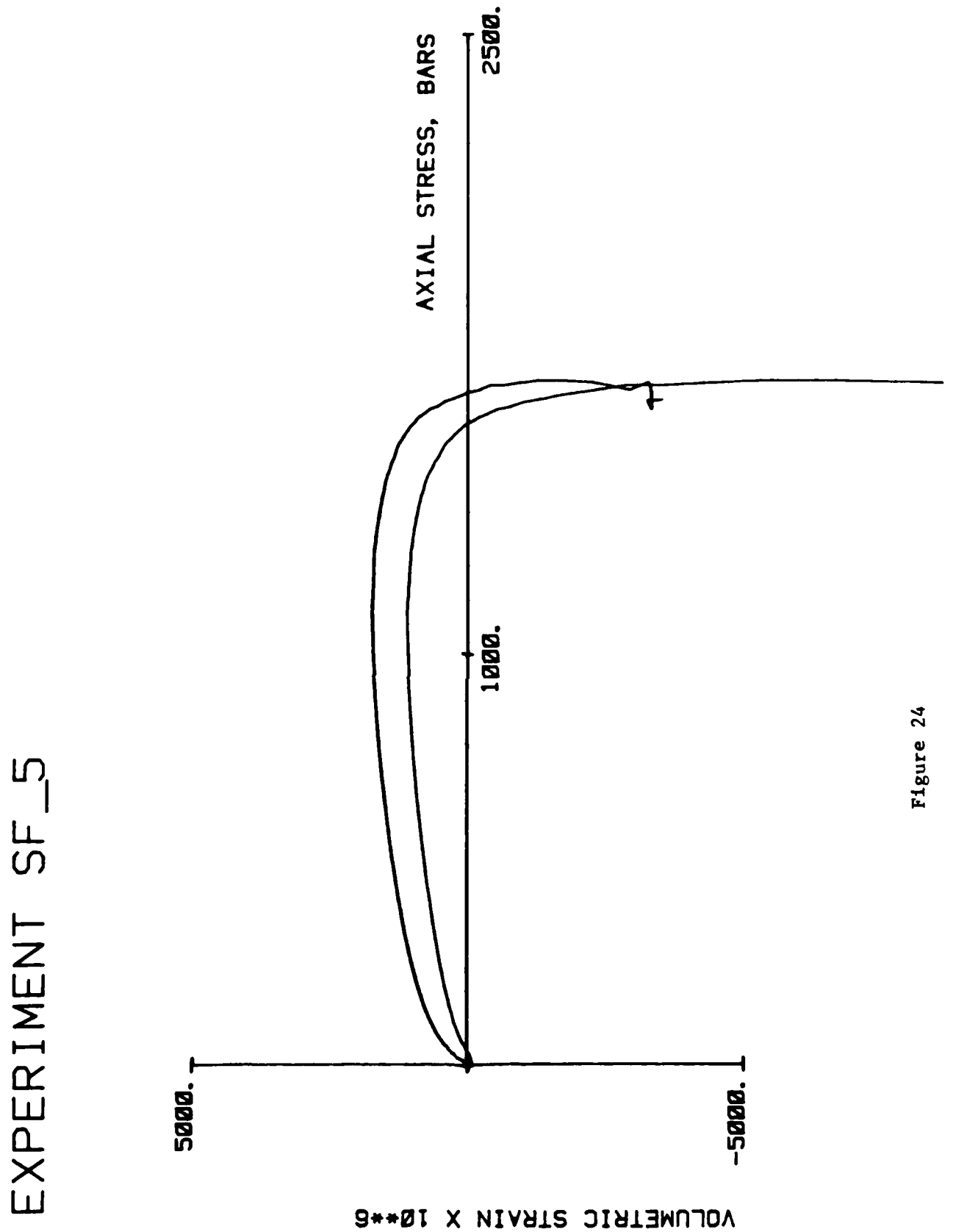
EXPERIMENT SF_5
AXIAL STRESS, BARS
2500.
1000.
5000.
-5000.
VOLUMETRIC STRAIN X 10**6

Figure 24

EXPERIMENT SF_5

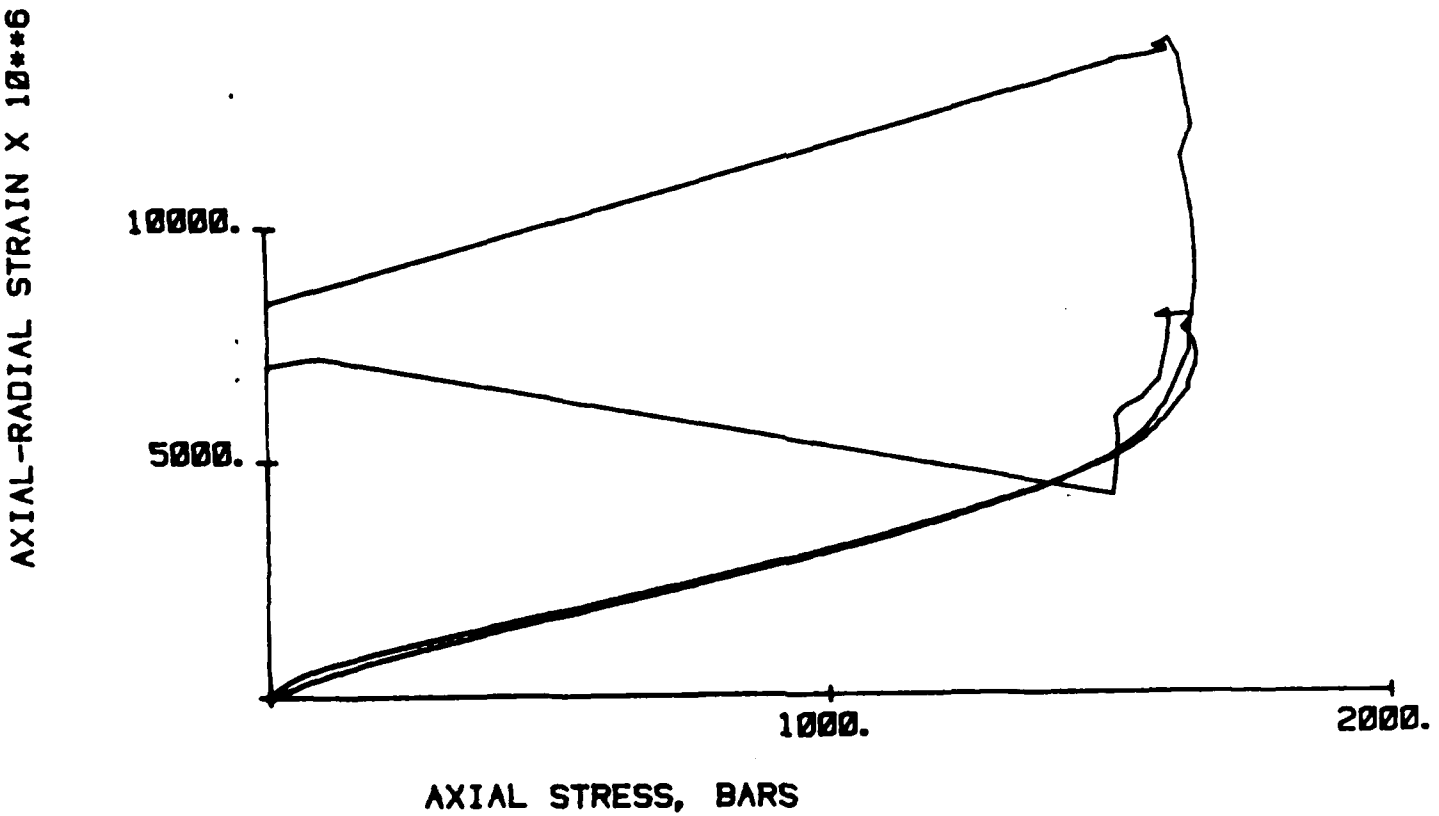

Figure 25

EXPERIMENT SF_6

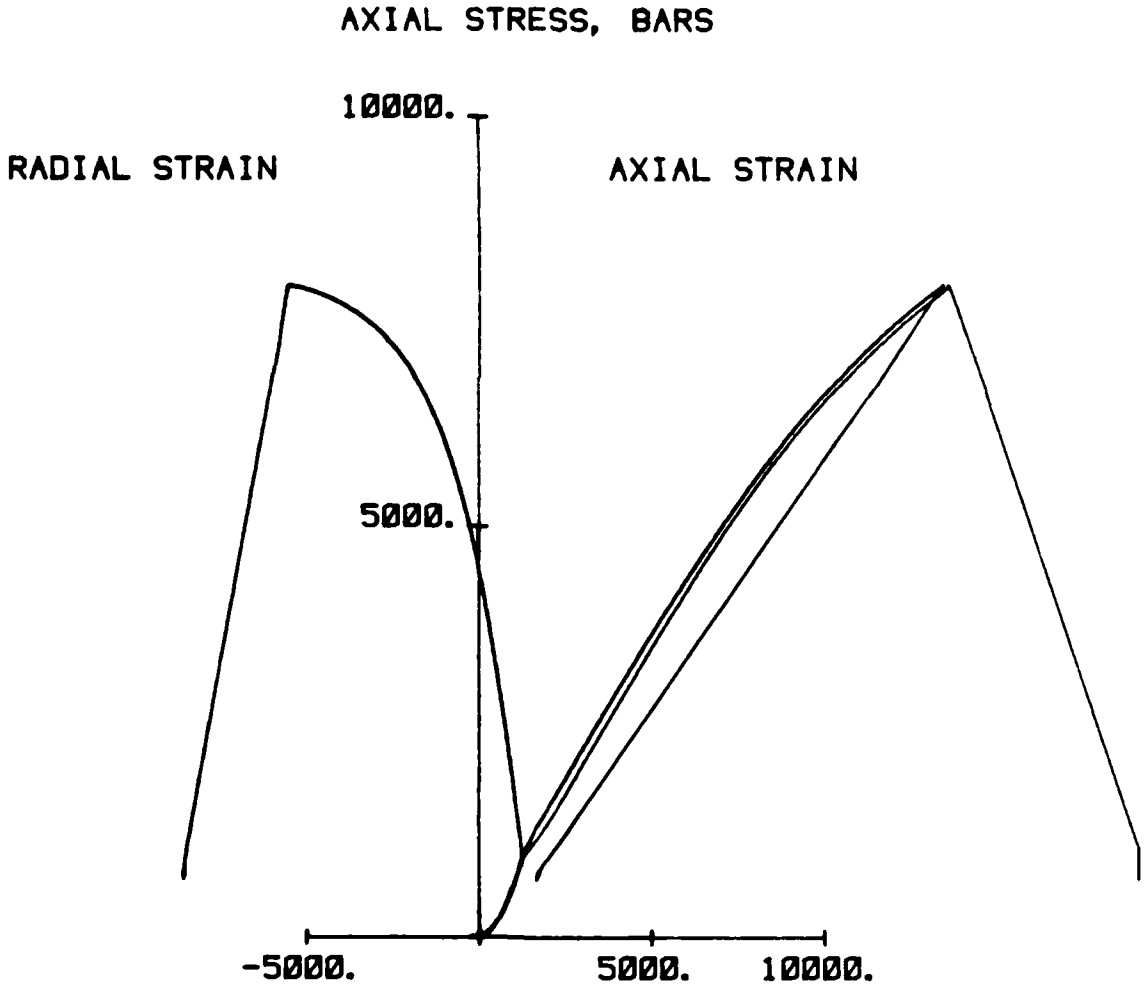

Figure 26

EXPERIMENT SF_6

VOLUMETRIC STRAIN VS AXIAL STRESS

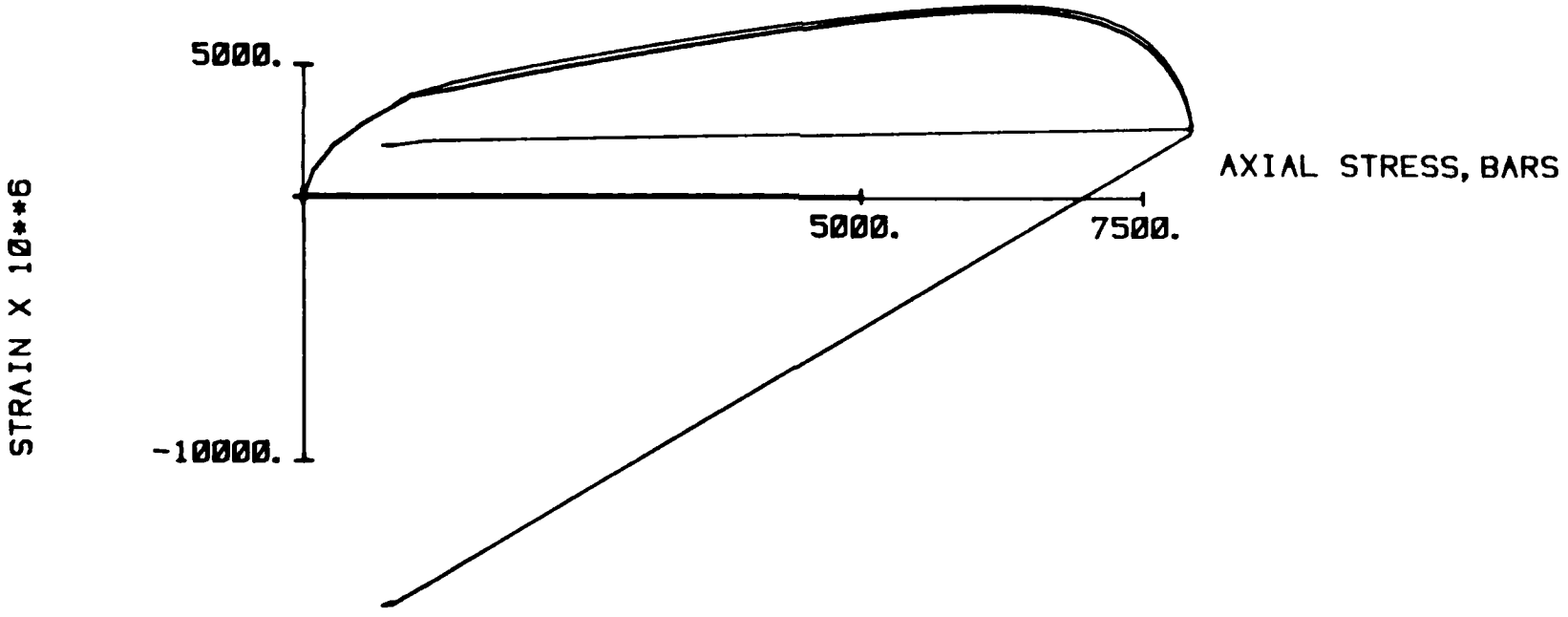

Figure 27

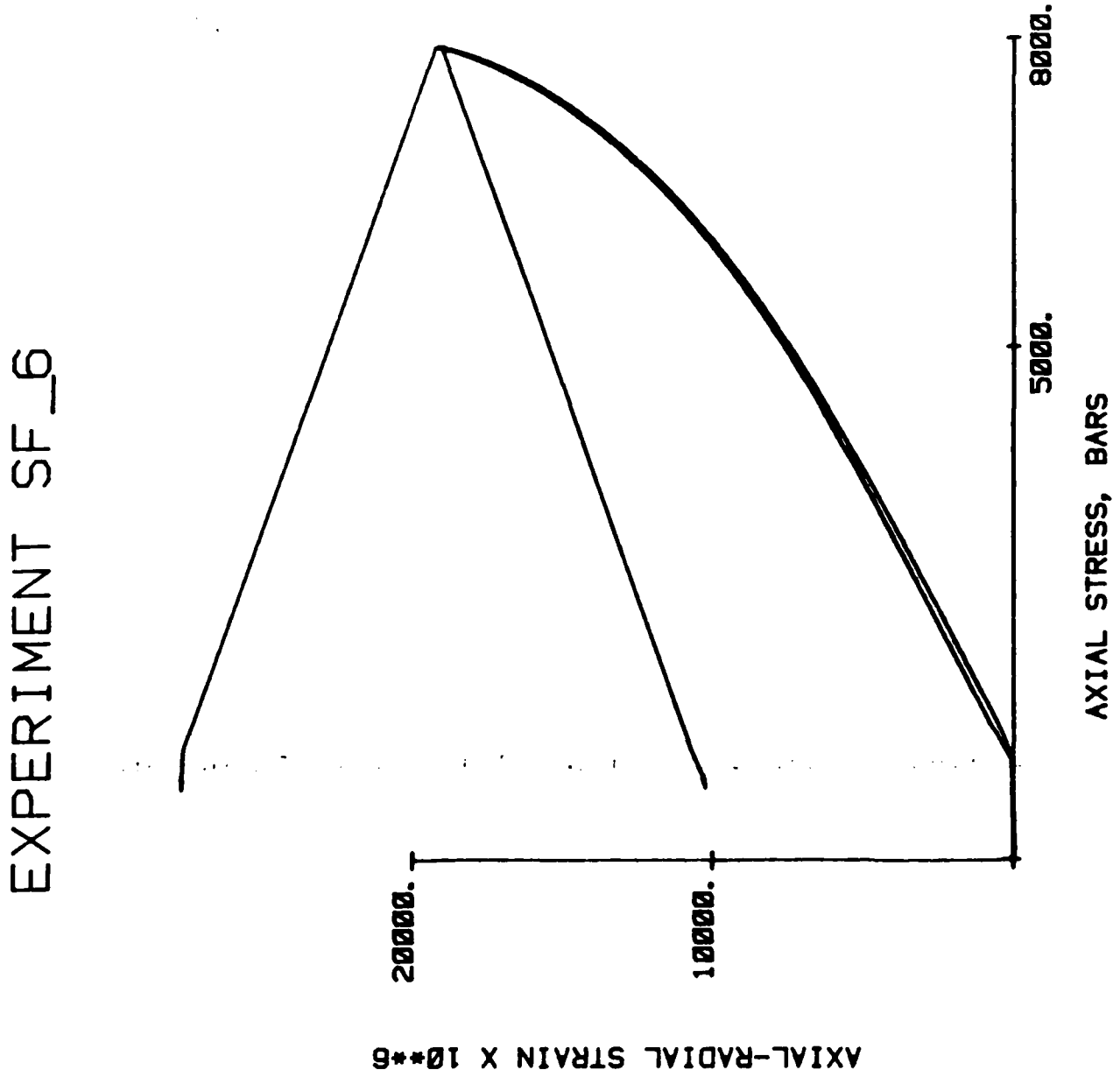
EXPERIMENT SF_6
AXIAL STRESS, BARS
8000.
5000.
20000.
10000.
AXIAL-RADIAL STRAIN X 10**6

Figure 28